HHS Public Access

Author manuscript

Pain. Author manuscript; available in PMC 2024 September 11.

Published in final edited form as:

Pain. 2024 April 01; 165(4): 866–883. doi:10.1097/j.pain.0000000000003080.

Targeted transcriptional upregulation of SENP1 by CRISPR activation enhances deSUMOylation pathways to elicit antinociception in the spinal nerve ligation model of neuropathic pain

Kimberly Gomez[a,b], **Heather N. Allen**[a,b], **Paz Duran**[a,b], **Santiago Loya-Lopez**[a,b], **Aida Calderon-Rivera**[a,b], **Aubin Moutal**[c], **Cheng Tang**[a,b], **Tyler S. Nelson**[a,b], **Samantha Perez-Miller**[a,b], **Rajesh Khanna**[a,b,d,*]

[a]Department of Molecular Pathobiology, College of Dentistry, New York University, New York, NY, United States

[b]NYU Pain Research Center, New York, NY, United States

[c]School of Medicine, Department of Pharmacology and Physiology, Saint Louis University, Saint Louis, MO, United States

[d]Department of Neuroscience and Physiology and Neuroscience Institute, School of Medicine, New York University, New York, NY, United States

Abstract

The voltage-gated sodium channel $Na_V1.7$ is an essential component of human pain signaling. Changes in $Na_V1.7$ trafficking are considered critical in the development of neuropathic pain. SUMOylation of collapsin response mediator protein 2 (CRMP2) regulates the membrane trafficking and function of $Na_V1.7$. Enhanced CRMP2 SUMOylation in neuropathic pain correlates with increased $Na_V1.7$ activity. Pharmacological and genetic interventions that interfere with CRMP2 SUMOylation in rodents with neuropathic pain have been shown to reverse mechanical allodynia. Sentrin or SUMO-specific proteases (SENPs) are vital for balancing SUMOylation and deSUMOylation of substrates. Overexpression of SENP1 and/or SENP2 in CRMP2-expressing cells results in increased deSUMOylation and decreased membrane expression and currents of $Na_V1.7$. Although SENP1 is present in the spinal cord and dorsal root ganglia, its role in regulating $Na_V1.7$ function and pain is not known. We hypothesized that favoring SENP1 expression can enhance CRMP2 deSUMOylation to modulate $Na_V1.7$ channels. In this study,

*Corresponding author. Address: Department of Molecular Pathobiology, College of Dentistry, New York University, 433 First Ave, 8th floor, New York, NY 10010, United States. rk4272@nyu.edu (R. Khanna).

Author contributions: R.K. developed the concept and designed the experiments. R.K. supervised experiments and advised on data analysis. K.G. and R.K. wrote the manuscript. T.S.N. and A.M. helped with editing the manuscript. A.M. designed the CRISPRa SENP1. K.G., A.C.-R., S.L.-L., and C.T. executed the electrophysiological recordings. P.D. performed biochemistry experiments. H.N.A. and T.S.N. performed RNAscope fluorescence in situ hybridization. K.G. performed the behavioral experiments. All authors had the opportunity to discuss the results and comment on the manuscript.

Supplemental digital content

Supplemental digital content associated with this article can be found online at http://links.lww.com/PAIN/B932.

Supplemental digital content is available for this article. Direct URL citations appear in the printed text and are provided in the HTML and PDF versions of this article on the journal's Web site (www.painjournalonline.com).

we used a clustered regularly interspaced short palindromic repeats activation (CRISPRa) SENP1 lentivirus to overexpress SENP1 in dorsal root ganglia neurons. We found that SENP1 lentivirus reduced CRMP2 SUMOylation, $Na_V1.7$–CRMP2 interaction, and $Na_V1.7$ membrane expression. SENP1 overexpression decreased $Na_V1.7$ currents through clathrin-mediated endocytosis, directly linked to CRMP2 deSUMOylation. Moreover, enhancing SENP1 expression did not affect the activity of TRPV1 channels or voltage-gated calcium and potassium channels. Intrathecal injection of CRISPRa SENP1 lentivirus reversed mechanical allodynia in male and female rats with spinal nerve injury. These results provide evidence that the pain-regulating effects of SENP1 overexpression involve, in part, the modulation of $Na_V1.7$ channels through the indirect mechanism of CRMP2 deSUMOylation.

Keywords

CRISPRa; SENP1; CRMP2; SUMO; $Na_V1.7$; Neuropathic pain

1. Introduction

Neuropathic pain, a chronic condition caused by somatosensory system damage or disease, involves upregulated proexcitatory ion channels such as $Na_V1.7$.[20] $Na_V1.7$ is a tetrodotoxin (TTX)-sensitive fast-activating and -inactivating channel[64] that amplifies subthreshold stimuli and contributes to the action potential's rising phase.[46] Mutations in *SCN9A*, which encodes $Na_V1.7$, are linked to various pain disorders, making it a significant contributor to pain signaling in humans. For example, $Na_V1.7$ gain-of-function causes severe pain in inherited erythromelalgia and paroxysmal extreme pain disorder, whereas $Na_V1.7$ loss-of-function produces congenital insensitivity to pain.[20]

$Na_V1.7$ is expressed at key sites of nociceptive transmission, including neurons of the dorsal root ganglia (DRG) and the dorsal horn of the spinal cord.[8] $Na_V1.7$ surface expression and current density are selectively controlled by SUMOylation—addition of a small ubiquitin-like modifier (SUMO) tag[37]—of the cytosolic phosphoprotein collapsin response mediator protein 2 (CRMP2).[23,24] When CRMP2 is not SUMOylated, it interacts with an endocytic machinery complex to promote clathrin-mediated endocytosis of $Na_V1.7$.[23,29] Accordingly, preventing the addition of SUMO to CRMP2 reduced $Na_V1.7$ currents and produced antinociception in rodents.[11,25] In addition, genetic interference of CRMP2 SUMOylation reversed mechanical allodynia in a rat model of neuropathic pain[51] and prevented the development of nerve injury–induced mechanical allodynia in mice.[49] Conversely, nerve injury increased CRMP2 SUMOylation with a commensurate increase in $Na_V1.7$ functional expression.[51] Thus, SUMOylation and deSUMOylation directly modulate $Na_V1.7$ expression and function to increase or attenuate neuropathic pain-like behavior, respectively.

Sentrin or SUMO-specific proteases (SENPs) are critical for maintaining the balance between SUMOylation and deSUMOylation. In addition to catalyzing the maturation process of SUMOs,[40] SENPs are also responsible for protein deSUMOylation. Mammals have at least 7 SENPs that differ in their subcellular localization and SUMO selectivity.[33] For example, SENP1 and SENP2 processes and deconjugate SUMO-1 and SUMO-2 and/or

SUMO-3, respectively.[63,66] We have previously shown that $Na_V1.7$ current density is reduced in cells that overexpress SENP1 and/or SENP2 in comparison to cells that express only wild-type CRMP2.[24] As both SUMO1 and SENP1 are expressed in spinal cord and DRG neurons,[73] we hypothesized that enhancing SENP1 expression would favor CRMP2 deSUMOylation to normalize $Na_V1.7$ channel-dependent excitability and contributions to neuropathic pain.

We report that increasing DRG *Senp1* expression using a clustered regularly interspaced short palindromic repeats activation (CRISPRa) SENP1 lentivirus (1) decreased CRMP2 SUMOylation, $Na_V1.7$–CRMP2 interaction, and $Na_V1.7$ membrane expression; (2) reduced $Na_V1.7$ (not TTX-resistant) currents through a clathrin-mediated endocytosis pathway; (3) did not further decrease sodium currents after pharmacological prevention of CRMP2 SUMOylation; and (4) decreased sensory neuron excitability. Furthermore, SENP1 overexpression did not affect native TRPV1 channels, voltage-gated calcium, or potassium channels. Intrathecal injection of CRISPRa SENP1 lentivirus reversed spinal nerve ligation–induced mechanical allodynia. Strikingly, this is the first study using CRISPRa to induce gene expression for treatment of chronic pain. Our results highlight the role of SENP1 as a mediator of CRMP2 deSUMOylation and SENP1 as a promising pharmacotherapeutic target for the modulation of $Na_V1.7$ activity to alleviate chronic pain.

2. Materials and methods

2.1. Animals

All experiments and procedures were performed in accordance with the guidelines recommended by the National Institutes of Health, the International Association for the Study of Pain, and the National Centre for the Replacement, Refinement, and Reduction of Animals in Research (NC3Rs) guidelines. Pathogen-free, adult female Sprague-Dawley rats (75–100 g; Charles River, Wilmington, MA) were used for RNAscope fluorescence in situ hybridization, western blot, and electrophysiological recordings of DRG neurons. Pathogen-free, adult male and female Sprague-Dawley rats (100–150 g; Envigo, Placentia, CA) were used for behavioral experiments. Animals were housed in the University of Arizona Laboratory Animal Research Center or New York University Kriser Dental Center Animal Facility in light (12-hour light: 12-hour dark cycle; lights on at 07:00 hours) and temperature (23 ± 3°C)-controlled rooms, with standard rodent chow and water ad libitum. The Institutional Animal Care and Use Committees of the College of Medicine at the University of Arizona and the College of Dentistry at the New York University approved all experiments.

2.2. Fluorescence in situ hybridization, imaging, and quantification

Rats were deeply anesthetized with isoflurane and euthanized through decapitation. Lumbar (L4 and L5) DRG were rapidly extracted using blunt dissection and frozen in optimal cutting temperature (OCT) on dry ice. Tissues were stored at −80°C until cryosectioning. Dorsal root ganglion tissue were cut to 20-μm thick sections on a cryostat, direct mounted on Superfrost Plus Microscope slides, and air dried overnight at room temperature (RT). The next morning slides underwent pretreatment for RNAscope fluorescence in situ

hybridization. First, the slides were dipped into distilled H_2O to remove OCT before a 15-minute bath in 10% neutral buffered formalin (4°C). Next, the slides were bathed for 5 minutes in 50% ethanol (RT), 5 minutes in 70% ethanol (RT), and then 10 minutes in 100% ethanol (RT). The slides were then dried for 5 minutes (RT), and a hydrophobic barrier was applied around each section using an ImmEdge hydrophobic barrier pen. Protease IV was applied to each section for 5 minutes (RT) in the humidity tray (Advanced Cell Diagnostics [ACD], EZ-Batch Slide Holder, Cat #: 321716) before beginning the RNAscope Fluorescent v2 assay (ACD, Cat #: 323110) and hybridization to marker probes. RNAscope probes used in this study were Rn-Calca-C2 (ACD, Cat#: 317511-C2), Rn-Senp1-C3 (ACD, Cat #: 1235591-C3), Rn-Nefh-C2 (ACD, Cat #: 474241-C2), and Rn-Scn9a-C1 (ACD, Cat#: 317851). The C1 channel (*Scn9a*) was labeled with Vivid Fluorophore 520 (ACD, Cat#: 323271), the C2 channel (*Calca* or *Nefh*) was labeled with TSA Vivid Fluorophore 650 (ACD, Cat#: 323273), and the C3 channel (*Senp1*) was labeled with TSA Vivid Fluorophore 570 (ACD, Cat#: 323272). All TSA Vivid Fluorophores were diluted at 1:1000. At the end of the RNAscope Fluorescent v2 assay, the slides received a 30-second DAPI incubation (RT) and were coverslipped with EverBrite Hardset Mounting Medium without DAPI (Cat#: 23003, Biotium, Fremont, CA). Stitched images encompassing an entire DRG section were captured on a Leica DMI8 microscope (Wetzlar, Germany) using a 40x objective and analyzed using QuPath software v0.4.3. Cells with at least 15 puncta (*Nefh*, *Calca*, and *Scn9a*) or 5 puncta (*Senp1*) associated with a DAPI nucleus were considered positive. Each individual dot represents the mean of 3 to 5 quantified sections across 2 DRG per individual rat. The final images were produced in Adobe Illustrator 2022.

2.3. *Overexpression of* Senp1 *with clustered regularly interspaced short palindromic repeats activation*

To activate the *Senp1* gene, we used a nuclease dead Cas9 (dCas9) fused to a tripartite activator, VP64-p65-Rta (VPR).[13] We obtained the SP-dCas9-VPR plasmid (Cat# 63798, Addgene, Watertown, MA)[13] and then subcloned the coding sequence for dCas9-VPR into pL-CRISPR.EFS.tRFP (Cat# 57819, Addgene)[32] in frame with the P2A-GFP sequences. This plasmid was further modified to eliminate, by silent mutations, 2 Esp3I restriction sites contained in the dCas9-VPR coding sequence. The resulting construct present the advantages of (1) having the ubiquitous core promoter for human elongation factor EF-1α driving the expression of dCas9-VPR, (2) having Cas9 fused to the self-cleavable P2A peptide followed by a tRFP to identify transfected or transduced cells, (3) expressing our guide RNA (gRNA) under the RNA polymerase III promoter for human U6 snRNA, and (4) containing the 5′ and 3′ long terminal repeat (LTR) from HIV-1 to be packaged in a lentivirus when needed. This novel all in one construct can be used to increase the transcription of genes of interest.

We designed a gRNA to increase the transcriptional activity of the SENP1 gene in rats; we identified the transcription starting site (TSS) at base 139684687 within the chromosome 7 (RefSeqID: NC_005106.4) of the genome build Rnor_6.0. We targeted the sequence from −100 to 0 bp from the TSS (139684587–139684687) with a gRNA (GAAAAAACCCCAGTCTGACA, on-score 70.4, off-score 35.8). The indicated gRNA sequence was inserted between the *Esp3I* restriction sites of our pL-

CRISPRA.EFS.tRFP lentiplasmid. The control plasmid consisted of a nontargeting gRNA (gGAGACGTGACCGTCTCT), GFP, and the dCas9-VPR. All cloning was performed by GenScript and plasmids were verified by Sanger sequencing (Eurofins, Louisville, KY).

2.4. Preparation of dissociated rat dorsal root ganglion neurons

Dorsal root ganglia from all levels were dissociated as described previously.[25,53] Female Sprague-Dawley rats (100–150 g) were euthanized according to institutionally approved procedures. In brief, lumbar DRG were collected, trimmed at their roots, and enzymatically digested in DMEM (Cat# 11965, Thermo Fisher Scientific, Waltham, MA) with neutral protease (3.125 mg/mL, Cat# LS02104, Worthington, Lakewood, NJ) and collagenase type I (5 mg/mL, Cat# LS004194, Worthington, Lakewood, NJ) for 50 minutes at 37°C under gentle agitation. The dissociated DRG neurons were gently centrifuged to collect cells and resuspended in complete DRG media [DMEM containing 1% penicillin and streptomycin sulfate from 10,000 μg/mL stock, 30 ng/mL nerve growth factor, and 10% fetal bovine serum (Hyclone, Logan, UT)]. Cells were seeded on poly-D-lysine–coated 12-mm coverslips or cell culture dishes.

2.5. Recombinant lentivirus production

Lentivirus particles containing pL-CRISPR-EFS-VPR-GFP or pL-CRISPR-EFS-VPR-GFP-SENP1 were packaged as described previously.[10] In brief, HEK293T cells were transfected with the plasmid vector system and the packaging plasmids to provide the VSV-G envelope. Two days posttransfection, the virus-containing medium was collected, and debris was removed by centrifugation. The virus was concentrated by ultracentrifugation, and the viral pellet was suspended in Dulbecco's modified Eagle's medium supplemented with 10% fetal bovine serum, passed through a 0.45-μm filter, and frozen at −80°C. The viral titer, as determined by analysis of the virus-associated p24 core protein (QuickTiter Lentivirus Quantitation Kit [Cell Biolabs, Inc, San Diego, CA]), was above 1×10^8 transducing units/mL for all viruses used in this study. Virus particles were produced in the University of Arizona Viral Production Core Facility.

2.6 Infection of dorsal root ganglion neurons

Adherent dorsal root ganglion cultures were infected with lentivirus particles (~1×10^6 IFU/mL) containing CRISPR-EFS-VPR-GFP-SENP1 or CRISPR-EFS-VPR-GFP. Sixteen hours after infection, media were replaced and cells were used for electrophysiological recordings, immunoblot analyses, and proximity ligation assays 2 days later.

2.7. Immunoblot preparation and analysis

Indicated samples were loaded on 4% to 20% Novex gels (Cat#: XP04205BOX; Thermo Fisher Scientific). Proteins were transferred for 1 hour at 100 V using TGS [25 mM Tris, pH 8.5, 192 mM glycine, and 0.1% (mass/vol) SDS], 20% (vol/vol) methanol as transfer buffer to polyvinylidene difluoride (PVDF) membranes (0.45 μm; Cat# IPFL00010; Millipore Sigma, St. Louis, MO), preactivated in pure methanol. After transfer, the membranes were blocked at room temperature for 1 hour with TBST (50 mM Tris·HCl, pH 7.4, 150 mM NaCl, and 0.1% Tween 20) with 5% (mass/vol) nonfat dry milk and

then incubated separately in indicated primary antibodies $Na_V1.7$ (Cat#: MA5–35253; Research Resource Identifiers [RRIDs]: AB_10808664; Thermo Fisher Scientific) and βIII-tubulin (Cat#: G7121; RRID: AB_430874; Promega, Madison, WI) in TBST, 5% (mass/vol) BSA, overnight at 4°C. After incubation in HRP-conjugated secondary antibodies from Jackson ImmunoResearch (West Grove, PA) (1/10,000 dilution), mouse anti-rabbit (Cat#: 211–032-171, RRID: AB_2339149), and goat anti-mouse (Cat#: 115–035-174, RRID:AB_2338512), blots were revealed by enhanced luminescence (Cat#: WBKLS0500; Millipore Sigma) before exposure to photographic film as described.[39]

2.8. Immunofluorescence, confocal microscopy, and quantification of $Ca_V2.2$ and $Na_V1.7$

Female rat DRG neurons in culture were infected with either CRISPR-EFS-VPR-GFP (as control) or CRISPR-EFS-VPR-GFP-SENP1 lentiviruses. Two days later, immunofluorescence was performed as described previously.[23,49] In brief, cells were fixed for 5 minutes using ice-cold methanol and allowed to dry at room temperature. Cells were rehydrated in phosphate-buffered saline (PBS) and incubated overnight with anti-$Ca_V2.2$ antibody (1/200; Cat# ACC-002, Alomone Labs, Jerusalem, Israel) or anti-$Na_V1.7$ antibody (1/200; Cat# MABN41, Sigma-Aldrich, St. Louis, MO) in PBS with 3% bovine serum albumin at 4°C. Cells were then washed 3 times in PBS and incubated with PBS containing 3% bovine serum albumin and secondary antibodies, Alexa 594 goat anti-mouse or Alexa 594 goat anti-rabbit (Thermo Fisher Scientific), for 1 hour at room temperature. After washing with PBS, cells were stained with 49,6-diamidino-2-phenylindole (DAPI, 50 mg/mL) and mounted in ProLong Diamond Antifade Mountant (Cat# P36961, Life Technologies Corporation, San Diego, CA). Immunofluorescent micrographs were acquired using a Plan Apochromat 63x/1.4 oil CS2 objective on a Leica SP8 confocal microscope operated by the LASX microscope software (Leica, Wetzlar, Germany). Camera gain and other relevant settings were kept constant. Membrane immunoreactivity was calculated by measuring the signal intensity in the area contiguous to the boundary of the cell. The membrane to cytosol ratio was determined by defining regions of interest in the cytosol and on the membrane of each cell using Image J. Total fluorescence was normalized to the area analyzed and before calculating the ratios.

2.9. Calcium imaging of rat dorsal root ganglion neurons

Changes in calcium influx in rat DRG neurons were determined as previously described.[22,50] Dorsal root ganglion neurons were loaded for 30 min at 37°C with 3 μM of Fura-2AM (Cat#: F1221, Thermo Fisher Scientific, stock solution prepared at 1 mM in DMSO with 0.02% Pluronic acid, Cat#: P-3000MP, Life Technologies) to see changes in intracellular calcium $[Ca^{2+}]_c$ in a standard Tyrode bath solution containing 139 mM NaCl, 3 mM potassium chloride (KCl), 0.8 mM $MgCl_2$, 1.8 mM $CaCl_2$, 5 mM glucose, and 10 mM Na HEPES (pH 7.4). To determine the changes in depolarization-induced calcium influx, baseline was acquired for 1 minute, then Ca^{2+} influx was stimulated with a 15-second pulse with an excitatory solution (40 or 90 mM KCl at ~310 mOsm). Cells were first examined under bright field to exclude those showing signs of lysis. To determine the contribution of T-type channels in response to the stimulus with 40 mM KCl, we used the selective blocker 3,5-dichloro-N-[1–(2,2-dimethyl-tetrahydro-pyran-4-ylmethyl)-4-fluoropiperidin-4-ylmethyl]-benzamide (TTA-P2, 1 μM) diluted in the standard

and excitatory solutions. To determine the changes in ligand-induced calcium influx, baseline was acquired for 1 minute, then Ca^{2+} influx was stimulated with a 15-second pulse with 200 nM capsaicin diluted in the standard Tyrode solution. Response was followed for 6 minutes while bath solution was continuously perfused over the cells to wash off excess of the trigger. This process was automated using the software WinTask ×64 (version 5.1, WinTask, Sector 3, Bucharest) that controlled the perfusion of the standard bath solution and triggers through ValveLink 8.2 software (Automate Scientific, Berkeley, CA). At the end of the protocol, cell viability was assessed by depolarization-induced Ca^{2+} influx using an excitatory 90 mM KCl solution. Fluorescence imaging was performed with an inverted microscope, Nikon Eclipse TE2000-U (New York, NY), using an objective Nikon Super Fluor 20 × 0.75 NA and a Photometrics cooled CCD camera Cool-SNAPHQ (Roper Scientific, Tucson, AZ) controlled by MetaFluor 6.3 software (Molecular Devices, Downingtown, PA). The excitation light was delivered by a Lambda-LS system (Sutter Instrument, Novato, CA). The excitation filters (340 ± 5 and 380 ± 7) were controlled by a Lambda 10 to 2 optical filter change (Sutter Instrument). Fluorescence was recorded through a 505-nm dichroic mirror at 535 ± 25 nm. To minimize phototoxicity and photobleaching, the images were taken every ~10 seconds during the time course of the experiment using the minimal exposure time that provided acceptable image quality. Changes in $[Ca^{2+}]_c$ were monitored by following a ratio of F340/F380, calculated after the subtraction of the background from both channels.

2.10. Proximity ligation assays

The proximity ligation assay (PLA) was performed as described previously[49,52,54] to visualize protein–protein interactions by microscopy. This assay is based on paired complementary oligonucleotide-labelled secondary antibodies that can hybridize and amplify a red fluorescent signal only when bound to 2 corresponding primary antibodies whose targets are in close proximity (within 30 nm). In brief, dorsal root ganglion neurons were fixed using ice-cold methanol for 5 minutes and allowed to dry at room temperature. The proximity ligation assay was performed according to the manufacturer's protocol using the Duolink Detection Kit with PLA PLUS and MINUS probes for mouse and rabbit antibodies (Duolink In Situ Detection Reagents Red, Cat.#: DUO92008; Duolink In Situ PLA Probe Anti-Rabbit MINUS, Cat #: DUO92005; and Duolink In Situ PLA Probe Anti-Mouse PLUS, Cat #: DUO92001, Sigma-Aldrich). Primary antibodies (1/1000 dilution) were incubated for 1 hour at RT; $Na_V1.7$ (Cat#: MABN41; Millipore, RRID:AB_10808664), CRMP2 (Cat#: C2993; Sigma-Aldrich, RRID:AB_1078573), SUMO1 (Cat#: S8070; Sigma-Aldrich, RRID:AB_477543), and CRMP2 (Cat#: 11096; Tecan, immunobiological lab, RRID:AB_494511). Cells were then stained with 49,6-diamidino-2-phenylindole (DAPI, 50 mg/mL) to detect cell nuclei and mounted in ProLong Diamond Antifade Mounting Medium (Cat#: P36961, Life Technologies Corporation). Immunofluorescent micrographs were acquired using a Plan Apochromat 63x/1.4 oil CS2 objective on a Leica SP8 confocal microscope operated by the LAS X microscope software (Leica). Camera gain and other relevant settings were kept constant throughout imaging sessions. Image J was used to count the number of PLA puncta per cell.

2.11. Electrophysiological recordings from rat dorsal root ganglion neurons

All recordings were performed using procedures adapted from our previous work.[53,59,77] Recordings were performed from acutely dissociated DRG neurons from Sprague-Dawley rats with a capacitance value below 30 pF, which has been historically associated with the population of small-diameter DRG neurons.[3]

For sodium current recordings, the internal pipette solution consisted of (in mM) 140 CsF, 10 NaCl, 1.1 Cs-EGTA, and 15 HEPES (pH 7.3, mOsm/L = 290–310) and external solution contained (in mM) 140 NaCl, 30 tetraethylammonium chloride, 10 D-glucose, 3 KCl, 1 $CaCl_2$, 0.5 $CdCl_2$, 1 $MgCl_2$, and 10 HEPES (pH 7.3, mOsm/L = 310–315). Dorsal root ganglion neurons were interrogated with current–voltage (I–V) and activation and inactivation voltage protocols. The voltage protocols were as follows: (1) I–V protocol: from a holding potential of −60 mV, cells were depolarized with 150-millisecond voltage steps over a range of −70 to +60 mV in +5 mV increments and (2) inactivation protocol: from a holding potential of −60 mV, cells were subjected to hyperpolarizing and repolarizing pulses for 1 second over a range of −120 to 0 mV in +10 mV steps. In experiments using **194**, this compound was added overnight at a final concentration of 5 μM. When $Na_V1.7$ blocker was used, ProTx-II was added into the external recording solution at a final concentration of 5 nM. When tetrodotoxin was used to isolate TTX-r currents, TTX was added into the external solution at a final concentration of 300 nM. In experiments where clathrin-mediated endocytosis was prevented with 20 μM Pitstop2,[70] the compound was added on the cells 30 minutes before the experiment.

For TRPV1 recordings, the external solution contained (in mM) 150 NaCl, 5 KCl, 2 $CaCl_2$, 1 $MgCl_2$, 10 glucose, and 10 HEPES (pH 7.4, mOsm/L = 300). The pipette solution for voltage-clamp experiments contained (in mM) 150 KCl, 5 $MgCl_2$, and 10 HEPES (pH 7.2, mOsm/L = 280).

Cells were placed in a perfusion chamber along with external solution flowing at 2 to 3 mL/minute from a peristaltic pump. TRPV1 currents were recorded by holding the membrane potential at −60 mV, and TRPV1-current amplitudes were evoked in response to perfusion of 1 μM of capsaicin. After reaching the maximum current amplitude after capsaicin, external solution was perfused. Bath solution exchange was essentially complete by <30 seconds.

To isolate potassium currents, the extracellular solution contained (in mM) 140 N-methyl-glucamine chloride, 5 KCl, 2 $CaCl_2$, 1 $MgCl_2$, 10 HEPES, and 10 glucose, pH adjusted to 7.4 with KOH. Recording pipettes were filled with the following solutions (in mM): 140 KCl, 5 $MgCl_2$, 4 ATP, 0.3 GTP, 2.5 $CaCl_2$, 5 EGTA, and 10 HEPES, adjusted pH at 7.3 with KOH. The membrane was held at −60 mV. To obtain I_KA, a 4-second prepulse to −100 mV was applied, followed by voltage steps of 500 milliseconds that ranged from −80 to +40 mV in +20-mV increments at 15-second intervals. I_KS was obtained from a conditioning 4-second prepulse to −40 mV, followed by voltage steps of 500 milliseconds that ranged from −80 to +40 mV in 120-mV increments at 15-second intervals. Inactivation of I_KA was determined by using a series of 4-second prepulses that ranged from −100 to −40 mV (10-mV increments) that were immediately followed by a 200-millisecond step to +60 mV. Inactivation of I_KS was determined by using a series of 4-second prepulses that ranged from

−100 to +20 mV (20-mV increments) that were immediately followed by a 200-millisecond step to +60 mV.

Normalization of currents to each cell's capacitance (pF) was performed to allow for collection of current density data. For sodium I–V curves, functions were fitted to data using a nonlinear least-squares analysis. I–V curves were fitted using double Boltzmann functions as follows:

$$f = a + g1/(1 + \exp((x - V_{1/2}1)/k1)) + g_2/(1 + \exp(-(x - V_{1/2}2)/k2))$$

where x is the prepulse potential, $V_{1/2}$ is the midpoint potential, and k is the corresponding slope factor for single Boltzmann functions. Double Boltzmann fits were used to describe the shape of the curve, not to imply the existence of separate channel populations. Numbers *1* and *2* simply indicate first and second midpoints; a along with g are fitting parameters.

Activation curves were obtained from the I–V curves by dividing the peak current at each depolarizing step by the driving force according to the equation: $G = I/(V_{mem} - E_{rev})$, where I is the peak current, V_{mem} is the membrane potential, and E_{rev} is the reversal potential. The conductance (G) was normalized against the maximum conductance (G_{max}). Activation curves were fitted with the Boltzmann equation as follows:

$$G/G_{max} = 1/[1 + exp(V_{0.5} - Vm)/k]$$

where G is the conductance in $G = I/(V_m - E_{Ca})$, G_{max} is the maximal conductance obtained from the Boltzmann fit under control conditions, $V_{0.5}$ is the voltage for half-maximal activation or inactivation, V_m is the membrane potential, and k is a slope factor.

Inactivation curves were obtained by dividing the peak current recorded at the test pulse by the maximum current (I_{max}). Steady-state inactivation (SSI) was fitted with the following equation:

$$I/I_{max} = 1/[1 + \exp(Vm - V_{0.5})/k]$$

where I is the current, I_{max} is the maximal current obtained from the Boltzmann fit under control conditions, $V_{0.5}$ is the voltage for half-maximal activation or inactivation, V_m is the membrane potential, and k is a slope factor.

Capacitive artifacts were fully compensated, and series resistance was compensated by ~70%. Recordings made from cells with greater than a 20% shift in series resistance compensation error were excluded from the analysis. All experiments were performed at room temperature (~23°C).

2.12. L5 and L6 spinal nerve ligation in rats

Male and female rats (~150 g) were deeply anesthetized with isoflurane (4% for induction and 2% for maintenance). The lower half of the animal's back was shaved. After surgical preparation, the left L5 and L6 spinal nerves were exposed by removing the paraspinal muscles and ligated with a 5–0 silk suture in a region distal to the DRG.[34] After hemostasis was confirmed, muscle and fascia were closed in layers using 5–0 absorbable suture, and the skin was closed with wound clips. Animals were allowed to recover for 14 days.

2.13. Intrathecal administration of lentiviruses for behavior

Lentivirus particles (~5×10^5 IFU/mL) containing CRISPR-EFS-VPR-GFP and CRISPR-EFS-VPR-GFP-SENP1 were injected intrathecally (15 μL) between L4 and L5 intervertebral level into isoflurane anesthetized rats (4% for induction and 2% for maintaining). In rats, 14 days after spinal nerve ligation, intrathecal injections of lentiviruses were performed, and behavior was measured 5 days after injection.

2.14. Measurement of mechanical allodynia

Mechanical allodynia was assessed by measuring rats' paw withdrawal threshold in response to probing with a series of fine calibrated filaments (von Frey, Stoelting, Wood Dale, IL). Rats were placed in suspended plastic cages with a wire mesh floor, and each von Frey filament was applied perpendicularly to the plantar surface of the paw. The "up–down" method (sequential increase and decrease of the stimulus strength) was used to determine the withdrawal threshold. The Dixon nonparametric method was used for data analysis, as described by Chaplan et al.[12] Data were expressed as the paw withdrawal threshold. Mechanical allodynia was manifested as a decrease in paw withdrawal threshold.

2.15. Identification of potential SENP1 activation (allosteric) sites

Representative SENP structures were aligned, prepared with the Schrödinger docking suite (Schrödinger, LLC, New York, NY, 2022), and analyzed with SiteMap.[30] All identified sites were visually examined, and only 1 was found to be unique to SENP1 and SENP2 isoforms. Representative structures in the uncomplexed state and complexed with pre-SUMO, mature SUMO, or SUMO and RanGAP1 were as follows: SENP1 PDB IDs 2iyc, 2iy1, 2iyd, 2iy0[66]; SENP2 1th0, 1tgz,[62] 2io0, 2io2[63]; SENP7 3eay,[44] 7r2e[42]; and NEDP1/SENP8 2bkq, 2bkr.[67]

2.16. Data Analysis

Graphing and statistical analysis was performed with (GraphPad Prism version 9.5). All data sets were checked for normality using the D'Agostino and Pearson test. Details of statistical tests, significance, and sample sizes are reported in the appropriate figure legends and in Supplementary Table 1 (available at http://links.lww.com/PAIN/B932). All data plotted represent mean ± SEM. RNAscope fluorescence in situ hybridization analysis was performed using the unpaired *t* test. Statistical differences for western blots, PLA, calcium imaging, and confocal experiments were determined by the Mann–Whitney test. For electrophysiological recordings, when 4 groups were compared, peak current densities were analyzed using 1-way ANOVA with Holm–Sidak post hoc test. When 2 groups were compared, peak current densities were analyzed by the Mann–Whitney test. $V_{1/2}$ midpoint

potentials, *k* slope factors, and conductances in Table 1 were compared using 1-way ANOVA with Tukey post hoc test and unpaired *t* test. Time constant (τ) of inactivation was compared using 2-way ANOVA with Holm–Sidak multiple comparison test and multiple *t* test. For the number of action potentials, rheobase, resting membrane potentials, and input resistance, the significance was analyzed by the Mann–Whitney test. Behavioral data were analyzed by 2-way ANOVA, followed by the Sidak multiple comparison test, and area under the curve with the Mann–Whitney test.

3. Results

3.1. Senp1 *is expressed in putative nociceptors*

First, we used multilabel fluorescence in situ *hybridization* (FISH) to neurochemically characterize *Senp1* expression in lumbar (L4-L5) DRG neurons from adult male and female rats (Fig. 1). We found that *Senp1* is widely distributed in peptidergic (*Calca*-expressing; 71.06 ± 3.217%), myelinated (*Nefh*-expressing; 52.85 ± 3.028%), and $Na_V1.7$-expressing (72.42 ± 2.645%) sensory neurons.

3.2. SENP1 overexpression using clustered regularly interspaced short palindromic repeats activation decreases collapsin response mediator protein 2 SUMOylation, CRMP2 binding, and $Na_V1.7$ membrane expression in dorsal root ganglion neurons

Next, we used a modified CRISPR approach (see the Methods section) to increase *Senp1* in DRG neurons to gain insight into the role of SENP1 in regulating CRMP2 SUMOylation and $Na_V1.7$ functional activity. As preventing SUMOylation of CRMP2 is antinociceptive,[11,23,49] we hypothesized that activating deSUMOylation would also achieve a similar outcome. We boosted the deSUMOylation machinery (*Senp1* expression) in DRG neurons using a CRISPRa SENP1 lentivirus. This CRISPR–Cas9 system uses a dead Cas9 (dCas9) whose endonuclease activity is removed through point mutations in its endonuclease domains, which is fused with transcriptional activators VP64 (composed of 4 tandem copies of the minimal activation domain of herpes simplex virus VP16),[5] p65[57] (transcriptional activation domain of human RelA), and Rta (transcriptional activation domain from the human herpesvirus) replication and transcription activator Rta/BRLF1,[13,31] named VPR.[13] We then generated a modified plasmid[32] to allow the expression of dCas9, GFP, and the programmable single guide RNA (sgRNA) to stimulate target gene expression. The sgRNA targets the −100 to 0 region (0 is the transcription start site, TSS) of the rat *Senp1* gene (Fig. 2A).

To validate that our CRISPRa strategy increases SENP1 expression, we generated a lentiplasmid and adherent DRG neuron cultures were infected with lentiviral particles (~1×10^6 IFU/mL) containing CRISPR-EFS-VPR-GFP (as control) or CRISPR-EFS-VPR-GFP-SENP1. Two days after infection, western blot analysis with a validated antibody against SENP1 was performed to test overexpression. A significant increase in SENP1 expression levels was observed in the CRISPR-EFS-VPR-GFP-SENP1–infected DRG compared with CRISPR-EFS-VPR-GFP–infected cells (CRISPR-EFS-VPR-GFP: 1.000 ± 0.023 a.u.; CRISPR-EFS-VPR-GFP-SENP1: 2.511 ± 0.424 a.u.; $P = 0.0079$; Figs. 2B,C and Table S1, available at http://links.lww.com/PAIN/B932).

To verify whether CRMP2 SUMOylation is impaired by SENP1 overexpression, we performed a proximity ligation assay (PLA) to detect SUMOylated CRMP2 in DRG neurons. Proximity ligation assay is a technique used to identify protein–protein interactions in situ with high specificity and sensitivity.[79] We stained DRG neurons using a CRMP2 and a SUMO1 antibody, followed by the PLA protocol (Fig. 3A). The number of PLA signals were then quantified per DRG neuron. We found that DRG neurons infected with CRISPR-EFS-VPR-GFP-SENP1 (~1×10^6 IFU/mL) showed a significant reduction in CRMP2 SUMOylation when compared to cells infected with CRISPR-EFS-VPR-GFP (CRISPR-EFS-VPR-GFP: 7.158 ± 0.631 PLA puncta per neuron; CRISPR-EFS-VPR-GFP-SENP1: 3.439 ± 0.328 PLA puncta per neuron; $P < 0.0001$; Fig. 3B and Table S1, available at http://links.lww.com/PAIN/B932). Similarly, using a CRMP2 and an $Na_V1.7$ antibody we tested whether overexpression of SENP1 affected $Na_V1.7$ binding to CRMP2 (Fig. 3C) and found that PLA puncta between $Na_V1.7$ and CRMP2 were reduced in cells transduced with CRISPR-EFS-VPR-GFP-SENP1 (CRISPR-EFS-VPR-GFP: 3.647 ± 0.452 PLA puncta per neuron; CRISPR-EFS-VPR-GFP-SENP1: 1.590 ± 0.216 PLA puncta per neuron; $P = 0.0002$; Fig. 3D and Table S1, available at http://links.lww.com/PAIN/B932).

Because uncoupling $Na_V1.7$ from CRMP2 can result in decreased $Na_V1.7$ trafficking to the plasma membrane,[11,49] we quantified the membrane expression levels of $Na_V1.7$ channels using confocal microscopy. Similar to the findings observed when preventing CRMP2 SUMOylation,[11,49] overexpression of SENP1 induced a noticeable reduction in surface localization of $Na_V1.7$ when compared to control neurons (CRISPR-EFS-VPR-GFP: 1.000 ± 0.029 a.u.; CRISPR-EFS-VPR-GFP-SENP1: 0.916 ± 0.027 a.u.; $P = 0.0385$; Figs. 3E–F and Table S1, available at http://links.lww.com/PAIN/B932).

Overall, these results validate our CRISPRa strategy to overexpress SENP1 and show that CRISPR-EFS-VPR-GFP-SENP1 does indeed attenuate CRMP2 SUMOylation, $Na_V1.7$–CRMP2 interaction, and $Na_V1.7$ surface localization in sensory neurons. Moreover, these data support our CRISPRa-induced SENP1 overexpression strategy for subsequent experiments.

3.3. Clustered regularly interspaced short palindromic repeats activation–mediated SENP1 overexpression leads to reduction of $Na_V1.7$ membrane expression and currents in sensory neurons

Having established that SENP1 overexpression reduces CRMP2 SUMOylation, disrupts $Na_V1.7$–CRMP2 interaction, and diminishes $Na_V1.7$'s surface expression in vitro, we sought to investigate whether the reduced $Na_V1.7$ membrane expression after overexpressing SENP1 correlates to a change in whole-cell Na^+ currents in small-sized DRG neurons. By using patch-clamp recordings, we found that infection of sensory neurons with CRISPR-EFS-VPR-GFP-SENP1 (~1×10^6 IFU/mL) decreased sodium currents (Fig. 4A) and current densities (Figs. 4B–C) by ~47% when compared to cells infected with CRISPR-EFS-VPR-GFP (CRISPR-EFS-VPR-GFP: −387.9 ± 58.69 pA/pF; CRISPR-EFS-VPR-GFP-SENP1: −206.7 ± 28.65 pA/pF; $P = 0.0414$; Fig. 4C and Table S1, available at http://links.lww.com/PAIN/B932). The conductance (G) was decreased in cells overexpressing SENP1 (Table 1). We observed no significant changes in voltage dependence of activation, steady-state

inactivation, and tau of inactivation between these 2 conditions (Fig. 4D and Tables 1 and 2). To interrogate the contribution of $Na_V1.7$ channels to the decrease in total sodium currents generated by SENP1 overexpression, we used protoxin-II (ProTx-II), a cystine knot peptide from tarantula venom known to inhibit the activation of $Na_V1.7$ channels by binding to VSD I, II, and IV.[9,65,76] We found that in cells infected with CRISPR-EFS-VPR-GFP, ~50% of the current was sensitive to ProTx-II (CRISPR-EFS-VPR-GFP: −366.0 ± 48.73 pA/pF; CRISPR-EFS-VPR-GFP + 5 nM ProTx-II: −187.6 ± 33.97 pA/pF; P = 0.0101; Fig. 4C and Table S1, available at http://links.lww.com/PAIN/B932). In other words, ~50% of the current was carried by $Na_V1.7$ channels. Conversely, addition of the $Na_V1.7$ blocker into cells infected with CRISPR-EFS-VPR-GFP-SENP1 did not further decrease sodium currents (CRISPR-EFS-VPR-GFP-SENP1: −204.8 ± 24.67 pA/pF; CRISPR-EFS-VPR-GFP-SENP1 + 5 nM ProTx-II: −186.2 ± 33.69 pA/pF; P = 0.9847; Fig. 4C and Table S1, available at http://links.lww.com/PAIN/B932). The conductance values were decreased in cells overexpressing SENP1 as well as those exposed to ProTx-II compared with control cells (Table 1). The voltage dependence of activation was shifted to the more depolarizing potentials by ~6 mV in the CRISPR-EFS-VPR-GFP + 5 nM ProTx-II group compared with cells treated with CRISPR-EFS-VPR-GFP alone (Fig. 4D and Table 1). This is consistent with previous findings of $Na_V1.7$ inhibition with ProTx-II.[76] Voltage dependence of inactivation and inactivation time constants were unaffected in these 2 conditions (Fig. 4D and Tables 1 and 2).

Adult rat DRG neurons also express tetrodotoxin-resistant (TTX-r; $Na_V1.8$ and 1.9) voltage-gated sodium channels.[19,26] To discard any potential effects of SENP1 overexpression in TTX-r currents, we isolated this slow and ultraslow inactivating currents by application of 300 nM of TTX (Figs. 4E,F). We found that cells infected with CRISPR-EFS-VPR-GFP-SENP1 + 300 nM TTX did not respond differently than cells transduced with CRISPR-EFS-VPR-GFP + 300 nM TTX (CRISPR-EFS-VPR-GFP + 300 nM TTX: −119.9 ± 20.52 pA/pF; CRISPR-EFS-VPR-GFP-SENP1 + 300 nM TTX: −131.9 ± 24.02 pA/pF; P = 0.4698; Fig. 4G and Table S1, available at http://links.lww.com/PAIN/B932). Voltage dependence of activation in CRISPR-EFS-VPR-GFP-SENP1–treated cells shifted ~5 mV to more positive potentials (Fig. 4H and Table 1). Steady-state inactivation did not differ significantly between the 2 conditions (Fig. 4H and Table 1) as well as inactivation time constants (Table 2). Altogether, these data underscore that among the voltage-gated sodium channels present in small-sized DRG neurons, $Na_V1.7$ channels, but not $Na_V1.8$ nor $Na_V1.9$, participate in sodium current reductions imposed by SENP1 overexpression. However, it is important to note that our findings do not exclude the possibility of SENP1 overexpression exerting effects on other ion channels expressed in these sensory neurons.

3.4. Sodium current reductions imposed by SENP1 overexpression are dependent on clathrin-mediated endocytosis

Trafficking of $Na_V1.7$ is reliant on clathrin-mediated endocytosis.[23,29] Non-SUMOylated CRMP2 forms a complex with the endocytic proteins Numb, Nedd4–2, and Eps15 to promote clathrin-mediated endocytosis of $Na_V1.7$[23,29]; therefore, we reasoned that blocking endocytosis may prevent sodium current density reductions imposed by SENP1 overexpression. To inhibit the formation of clathrin-coated pits, we used Pitstop2 (20 μM,

30 minutes)[29,70] and found that incubating sensory neurons with Pitstop2 had no effect on sodium currents in cells infected with CRISPR-EFS-VPR-GFP (CRISPR-EFS-VPR-GFP: −323.1 ± 51.09 pA/pF; CRISPR-EFS-VPR-GFP + 20 μM Pitstop2: −271.9 ± 29.88 pA/pF; $P = 0.7923$; Figs. 5A–C and Table S1, available at http://links.lww.com/PAIN/B932). Conversely, in cells transduced with CRISPR-EFS-VPR-GFP-SENP1, inhibiting clathrin coat assembly with Pitstop2 prevented sodium current reductions induced by overexpression of SENP1 (CRISPR-EFS-VPR-GFP-SENP1: −146.3 ± 25.75 pA/pF; CRISPR-EFS-VPR-GFP-SENP1 + 20 μM Pitstop2: −323.9 ± 64.04 pA/pF; $P = 0.0391$; Figs. 5A–C and Table S1, available at http://links.lww.com/PAIN/B932). The conductance value of cells overexpressing SENP1 was decreased to control cells (Table 1). No changes in the activation and inactivation's voltage dependence nor inactivation time constants were observed between these 4 groups (Fig. 5D and Tables 1 and 2). These findings support the role of clathrin-mediated endocytosis as a possible explanation for decreased sodium currents caused by overexpressing SENP1.

3.5. SENP1 controls CRMP2 deSUMOylation to modulate $Na_V1.7$ channel activity

Our previous work identified a small molecule named **194** (benzoylated 2-(4-piperidinyl)-1,3-benzimidazole analog; molecular weight 567.6) as a pharmacological tool to prevent CRMP2 SUMOylation by interfering with the interaction between E2 SUMO–conjugating enzyme Ubc9 and CRMP2.[11] We found that this compound selectively reduces $Na_V1.7$ surface expression and function and has antinociceptive effects in rodents.[11] Therefore, to test whether overexpression of SENP1 and compound **194** share a convergent mechanism of modulation (CRMP2 deSUMOylation), we next sought to explore the functional consequences of increasing SENP1 expression in the presence of **194**. We first found that adding compound **194** (5 μM, overnight) to sensory neurons infected with CRISPR-EFS-VPR-GFP inhibited sodium currents and current densities by ~64% (CRISPR-EFS-VPR-GFP: −343.6 ± 54.36 pA/pF; CRISPR-EFS-VPR-GFP + 5 μM **194**: −122.8 ± 46.32 pA/pF; $P = 0.0020$; Figs. 6A–C), which correlates with our previous findings.[11] Lack of further inhibition on coincubation of **194** in cells infected with CRISPR-EFS-VPR-GFP-SENP1 suggests that 100% of functional $Na_V1.7$ was blocked when overexpressing SENP1 (CRISPR-EFS-VPR-GFP-SENP1: −153.3 ± 54.36 pA/pF; CRISPR-EFS-VPR-GFP-SENP1 + 5 μM **194**: −148.1 ± 26.19 pA/pF; $P = 0.9412$; Figs. 6A–C and Table S1, available at http://links.lww.com/PAIN/B932). The conductance values of cells overexpressing SENP1 and those treated with **194** were reduced compared with untreated control cells (Table 1).Voltage dependence and tau of inactivation were unchanged in these 4 conditions (Fig. 6D and Tables 1 and 2). **194** caused a negative ~10 mV shift in the $V_{1/2}$ of inactivation in cells treated with CRISPR-EFS-VPR-GFP (Fig. 6D and Table 1), which is also consisted with our previous report.[11] These results suggest that SENP1 and compound **194** share a convergent mechanism of action, which is reducing CRMP2 SUMOylation to control $Na_V1.7$ channel function.

3.6. SENP1 overexpression attenuates dorsal root ganglion neuron excitability

Given that Na 1.7 channels (1) are indispensable for action potential (AP) electrogenesis[6] and (2) are critical for physiological and pathological pain,[20] we performed patch-

clamp recordings in DRG to further understand the consequences underlying SENP1 overexpression. We hypothesized that overexpressing SENP1 could suppress AP firing in sensory neurons. Of note, DRG excitability was measured by injecting a current ramp from 0 to 120 pA in 1 second into the soma of small-diameter DRG neurons to elicit APs (Fig. 7A). Representative traces (Fig. 7A) and plotted data (Fig. 7B) revealed that the number of evoked APs was significantly reduced in cells infected with CRISPR-EFS-VPR-GFP-SENP1 when compared to cells treated with CRISPR-EFS-VPR-GFP (CRISPR-EFS-VPR-GFP: 7.75 ± 0.79 APs; CRISPR-EFS-VPR-GFP-SENP1: 4.66 ± 1.02 APs; $P = 0.0496$; Fig. 7B and Table S1, available at http://links.lww.com/PAIN/B932). Similarly, the minimum current necessary to evoke an AP (rheobase) was increased after overexpression of SENP1 (CRISPR-EFS-VPR-GFP: 22.50 ± 3.55 pA; CRISPR-EFS-VPR-GFP-SENP1: 48.33 ± 8.33 pA; $P = 0.0157$; Fig. 7C and Table S1, available at http://links.lww.com/PAIN/B932). Moreover, the resting membrane potential (RMP; CRISPR-EFS-VPR-GFP: −44.00 ± 1.77 mV; CRISPR-EFS-VPR-GFP-SENP1: −40.33 ± 0.66 mV; $P = 0.1515$; Fig. 7D and Table S1, available at http://links.lww.com/PAIN/B932) and input resistance (CRISPR-EFS-VPR-GFP: 140.1 ± 8.29 MΩ; CRISPR-EFS-VPR-GFP-SENP1: 133.9 ± 16.35 MΩ; $P = 0.1515$; Fig. 7E and Table S1, available at http://links.lww.com/PAIN/B932) were equivalent in these 2 conditions. These observations show that somatic excitability of sensory neurons is indeed impaired after favoring SENP1 expression.

3.7. SENP1 overexpression does not affect the activity of TRPV1 channels, voltage-gated potassium, or voltage-gated calcium channels

The decrease in excitability observed in DRG neurons cannot be solely attributed to SENP1-mediated CRMP2 deSUMOylation because other ion channels can also undergo SUMOylation and deSUMOylation and contribute to increased excitability in pain conditions.[1] To explore potential off-target effects of SENP1 overexpression, we focused on TRPV1 channels, voltage-gated potassium, and voltage-gated calcium channels, which are known to be directly or indirectly modulated by SUMOylation.

In sensory neurons, native TRPV1 channels undergo SUMOylation by Ubc9[1] and deSUMOylation by SENP1.[73] Previous studies have shown that conditional deletion of Ubc9 in DRG neurons decreases capsaicin-evoked Ca^{2+} transients and Ca^{2+}currents,[1] whereas the elimination of SENP1 in DRG exacerbates thermal hyperalgesia through deSUMOylation of TRPV1.[73] To further explore the impact of SENP1 overexpression on TRPV1 channel activity, we used 2 distinct experimental approaches. First, we conducted Fura-2 ratiometric Ca^{2+} imaging experiments in DRG neurons to assess the changes in calcium response on capsaicin stimulation (200 nM). We observed no significant alteration in calcium response between cells transduced with CRISPR-EFS-VPR-GFP-SENP1 and the control group (CRISPR-EFS-VPR-GFP: 0.091 ± 0.008 arbitrary units (a.u); CRISPR-EFS-VPR-GFP-SENP1: 0.100 ± 0.014 a.u.; $P = 0.8763$; Supplementary Figure 1A and B and Table S1, available at http://links.lww.com/PAIN/B932). Second, we performed patch-clamp recordings in DRG neurons perfused with 1 μM of capsaicin. The results demonstrate that both TRPV1 currents and current densities remained unchanged in DRG neurons infected with CRISPR-EFS-VPR-GFP-SENP1, compared with those expressing the control lentivirus (CRISPR-EFS-VPR-GFP: 14.34 ± 3.35 pA/pF; CRISPR-EFS-VPR-GFP-SENP1: 17.52 ±

1.91 pA/pF; $P = 0.1893$; Supplementary Figure 1C and D and Table S1, available at http://links.lww.com/PAIN/B932). In addition, the deactivation time constant of TRPV1 currents was measured, and no significant differences were found between the tested conditions (CRISPR-EFS-VPR-GFP: 96.26 ± 20.37 seconds; CRISPR-EFS-VPR-GFP-SENP1: 86.26 ± 20.10 seconds; $P = 0.6730$; Supplementary Figure 1E and Table S1, available at http://links.lww.com/PAIN/B932).

Voltage-gated potassium channels are also subject to SUMOylation, a regulatory process that influences their surface expression, activity, kinetics, and voltage dependence of inactivation.[7,17,75] Both SENP1 and SENP2 have been identified as mediators of their deSUMOylation.[7,17,75] To investigate the impact of SENP1 overexpression on the functional activity and voltage dependence, we conducted voltage-clamp experiments focusing on rapidly inactivating $I_K A$ and slowly inactivating $I_K S$ potassium currents in DRG. The data obtained from these experiments revealed that the presence of overexpressed SENP1 in DRG did not lead to any significant differences in $I_K A$ currents (Supplementary Figure 2A, available at http://links.lww.com/PAIN/B932), current densities (Supplementary Figure 2B, available at http://links.lww.com/PAIN/B932), nor voltage dependence of activation (Supplementary Figure 2C, available at http://links.lww.com/PAIN/B932) and inactivation (Supplementary Figure 2D, available at http://links.lww.com/PAIN/B932) when compared to DRG infected with the control lentivirus (Table S1, available at http://links.lww.com/PAIN/B932). Similarly, when assessing slowly inactivating potassium currents, we obtained similar results indicating that overexpression of SENP1 does not alter the behavior of $I_K S$ currents (Supplementary Figure 2E-H and Table S1, available at http://links.lww.com/PAIN/B932).

A recent study reported that heterologously expressed high-voltage–activated $Ca_V 2.2$ calcium channels can be activated through SUMOylation mediated by Ubc9.[68] However, the activity of $Ca_V 2.2$ channels does not seem to be influenced by the coexpression of SENP1.[68] To confirm whether this observation holds true in a native system, we conducted Fura-2 ratiometric Ca^{2+} imaging experiments in DRG neurons. On depolarization with 90 mM KCl, which enables assessment of high-voltage–activated calcium channels, we observed that the calcium responses in cells infected with CRISPR-EFS-VPR-GFP-SENP1 did not show significant changes compared with control cells (CRISPR-EFS-VPR-GFP: 0.179 ± 0.011 a.u; CRISPR-EFS-VPR-GFP-SENP1: 0.233 ± 0.020 a.u; $P = 0.0823$; Supplementary Figure 3A and B and Table S1, available at http://links.lww.com/PAIN/B932). Although there was a tendency of the calcium response to increase in the presence of SENP1, the difference did not reach statistical significance. To further investigate potential alterations of $Ca_V 2.2$ channel membrane expression by SENP1 overexpression, we examined the surface localization of $Ca_V 2.2$. Our findings indicated that the surface expression of these channels remained unchanged between conditions (CRISPR-EFS-VPR-GFP: 1.00 ± 0.04 a.u; CRISPR-EFS-VPR-GFP-SENP1: 1.04 ± 0.05 a.u; $P = 0.6047$; Supplementary Figure 3C and D and Table S1, available at http://links.lww.com/PAIN/B932).

Another study demonstrated that USP5 (or isopeptidase T) SUMOylation can regulate $Ca_V 3.2$–USP5 interaction in DRG, leading to indirect modulation of low-voltage–activated $Ca_V 3.2$ calcium channels.[27] To investigate the activity of these channels, we performed

additional Fura-2 ratiometric Ca^{2+} imaging experiments in DRG neurons. Through depolarization with 40 mM KCl, which allows us to assess the activity of low-voltage–activated calcium channels, we examined the calcium responses in cells infected with CRISPR-EFS-VPR-GFP-SENP1 and compared them with control cells. The results show that there were no significant changes in the calcium responses between the 2 conditions (CRISPR-EFS-VPR-GFP: 0.264 ± 0.040 a.u; CRISPR-EFS-VPR-GFP-SENP1: 0.203 ± 0.018 a.u; $P = 0.4190$; Supplementary Figure 3E and F and Table S1, available at http://links.lww.com/PAIN/B932). We confirmed the response of Ca_V3 channels by using the channels' selective blocker, TTA-P2 (Supplementary Figure 3E and F, available at http://links.lww.com/PAIN/B932).

The findings imply that while SUMOylation is established in controlling TRPV1, I_KA and I_KS potassium channels, and $Ca_V2.2$ and $Ca_V3.2$ calcium channels, the absence of alterations due to SENP1 overexpression suggests the role of additional SENPs in modulating TRPV1, potassium, and calcium channels in this scenario.

3.8. CRISPR activation–mediated overexpression of SENP1 culminates in reversal of pain-like behaviors induced by spinal nerve ligation

We have shown above that facilitating SENP1 expression results in decreased $Na_V1.7$ membrane expression, sodium currents (mainly $Na_V1.7$ dependent), and DRG excitability. To support the involvement of SENP1 in pain in vivo, we next tested the relevance of this protease in a model of neuropathic pain induced by spinal nerve ligation (SNL).[34] Baseline (BL) measurements of mechanical allodynia were performed before SNL surgeries in female (Fig. 8A) and male (Fig. 8B) rats. Ligation of L5 and L6 spinal nerves resulted in the development of mechanical allodynia (Figs. 8A–B) 14 days after SNL (SNL time point). Next, rats were injected intrathecally (i.t.) into L4 and L5 intervertebral space with CRISPR-EFS-VPR-GFP and CRISPR-EFS-VPR-GFP-SENP1 (~5×10^5 IFU/mL live particles in 15 μL) and paw withdrawal thresholds and area under the curves (Figs. 8A–D) were measured 1, 2, 3, and 4 weeks postinjection. As shown in Figures 8A–C, i.t injection of CRISPR-EFS-VPR-GFP-SENP1 partially reversed SNL-induced mechanical allodynia in female rats 1 week after lentiviral injections (AUC of CRISPR-EFS-VPR-GFP: 3.47 ± 1.05; CRISPR-EFS-VPR-GFP-SENP1: 10.13 ± 0.88; $P = 0.0022$; Fig. 8C and Table S1, available at http://links.lww.com/PAIN/B932). Similarly, when compared to rats treated with CRISPR-EFS-VPR-GFP, male rats injected with CRISPR-EFS-VPR-GFP-SENP1 showed a significant reversal of mechanical allodynia 1 to 3 weeks after lentiviral injections (AUC of CRISPR-EFS-VPR-GFP: 9.39 ± 2.52; CRISPR-EFS-VPR-GFP-SENP1: 21.75 ± 3.27; $P = 0.01522$; Fig. 8D and Table S1, available at http://links.lww.com/PAIN/B932). These results suggest that increasing SENP1 expression is sufficient to reverse mechanical allodynia induced by spinal nerve injury. In addition, these findings support the use of CRISPRa gene-editing tool for treatment of neuropathic pain.

4. Discussion

The modulation of $Na_v1.7$ for therapeutic intervention in chronic pain conditions is an area of intense research focus. Unfortunately, multiple compounds targeting $Na_v1.7$ have

failed in recent clinical trials.[41,56] Multiple theories underlie the difficulty or failure to pharmacologically target $Na_v1.7$, but undeniably a key determinant is the challenge to selectively target this channel without affecting other similar channels in the nervous system. In contrast to pharmacologically targeting the $Na_v1.7$ channel directly, we have demonstrated that indirect regulation of $Na_v1.7$, through preventing the addition of SUMO1 onto the $Na_v1.7$ interacting protein CRMP2, blocked $Na_v1.7$ functions and was antinociceptive.[11,23,25,51] In this study, we built on these results and used a novel strategy that leverages the power of CRISPR activation to overexpress the deSUMOylation machinery (SENP1) and thereby to indirectly regulate $Na_v1.7$ in chronic pain. We report that in primary sensory neurons enhancing SENP1 expression by using CRISPRa reduced (1) CRMP2–SUMO1 and the $Na_V1.7$–CRMP2 interaction, (2) $Na_V1.7$ surface expression and currents (an effect that was mediated by clathrin-mediated endocytosis), (3) neuronal excitability, and (4) neuropathic pain-like behaviors in male and female rats (Fig. 9), without affecting the activity of TRPV1 channels nor voltage-gated calcium and potassium channels.

SUMOylation is a reversible posttranslational modification of lysine residues in proteins by small ubiquitin-like modifiers (SUMOs). Sentrin or SUMO-specific proteases are responsible for catalyzing SUMO maturation[40] and deSUMOylation, maintaining a balance between the 2 processes. Wang et al.[73] reported SENPs' involvement in pain and highlighted that SENP1 prevents increased sensitivity to heat in TRPV1 channels by maintaining decreased SUMOylation. Peripheral inflammation enhances protein SUMOylation in DRG, and conditional SENP1 knockout worsens thermal hyperalgesia in inflammatory pain models. SENP1's role in inflammation has also been supported by other studies.[73] For instance, lipopolysaccharide (LPS)-induced inflammatory response is dependent on SENP1 activation of the transcription factor Sp3 expression through its deSUMOylation.[78] Similarly, SENP1 seems to maintain low SUMOylation levels of peroxisome proliferator-activated receptor gamma (PPARγ) to mitigate microglia-mediated neuroinflammation.[72] These lines of evidence triangulate to demonstrate that SENP1 is needed for controlling pain and inflammation.

SUMOylation of proteins can affect their localization, activity, and interaction with other proteins.[36] For example, CRMP2's interaction and regulation of $Na_V1.7$ channels depends on its SUMOylation state.[23,24] Collapsin response mediator protein 2 SUMOylation has reported to be necessary for neuropathic pain[51] for the reason that when CRMP2 is SUMOylated, it interacts with $Na_V1.7$ channels to promote their membrane localization and function and maintain chronic pain.[23,24] However, when CRMP2 SUMOylation is decreased either by overexpression of SENP1,[24] genetically through mutation of its SUMOylation site (K374A),[49,51] or pharmacologically through the CRMP2 SUMOylation inhibitor **194**,[11] CRMP2 interacts with an endocytic complex formed by Numb, Nedd4–2, and Eps15 to enhance $Na_V1.7$ clathrin-mediated endocytosis.[23,29] Thus, preventing CRMP2 SUMOylation and subsequent positive regulation of $Na_V1.7$ channels has demonstrated to be a useful strategy to target pain[11,23,49] due to the major involvement of these channels in many pain-related conditions.

To study the role of CRMP2 deSUMOylation by SENP1, we used a CRISPRa strategy to overexpress SENP1 in adult rodents because germline deletion of SENP1 in mice causes

anemia and embryonic lethality.[15] Clustered regularly interspaced short palindromic repeats activation technology has many advantages over other strategies[4] including that it uses the endogenous regulatory elements to upregulate existing functional gene copy numbers with little to no off-target effects in vivo. [38,43,45] In vivo CRISPR-mediated gene activation has therapeutic benefits for many genetic or acquired diseases including muscular dystrophy,[38] epilepsy,[16] cancer,[71] Parkinson,[28] and myocardial infarction,[48] among others. Lentivirus-based CRISPR-dCas9 activator systems have been successfully used in neurons in vitro and in vivo, [18] thus supporting the use of our CRISPRa SENP1 lentivirus strategy. Importantly, to the best of our knowledge, the present work is the first to use the CRISPRa system to induce gene expression for the treatment of experimentally induced chronic pain. Although successful overexpression of cannabinoid type 1 (CB1) receptors (important players in analgesia) in neurons has been reported by the Ledri laboratory,[18] its connection to pain was never investigated.

Our results demonstrate that CRISPRa can be successfully used to overexpress genes involved in pain regulation and may potentially represent a next-generation gene therapy approach to treat chronic pain disorders. An example of a condition that could potentially benefit from the CRISPRa strategy is neurofibromatosis type 1 (NF1), a rare autosomal disorder that is associated with chronic idiopathic pain.[51] In NF1, haploinsufficiency results in a reduced level of wild-type (WT) neurofibromin in $Nf1^{+/-}$ cells, but introducing WT neurofibromin into $Nf1^{+/-}$ fibroblasts in vitro has been shown to reverse the cellular effects of NF1 haploinsufficiency.[47] Thus, normalizing the levels of WT neurofibromin with CRISPRa in NF1-haploinsufficient cells could be a potential strategy for treatment of NF1. Precedence for this already exists as CRISPRa has been used for other diseases associated with haploinsufficiency.[45] For instance, CRISPRa-recombinant adenoassociated virus injected into the hypothalamus led to reversal of the obesity phenotype in single-minded 1 (Sim1) and melanocortin 4 receptor (Mc4r) haploinsufficient mice.[45]

While interrogating the mechanisms underlying pain related to NF1, we and others found (1) increased sensory neuron excitability in *Nf1*$^{+/-}$ mice[74] and (2) increased expression and function of $Na_V1.1$, $Na_V1.7$, and $Na_V1.8$,[35,74] and $Ca_V2.2$[21] channels in rats with CRISPR-Cas9 editing of *Nf1*.[55] Subsequently, we discovered that CRMP2 was involved in this regulation[58] because neurofibromin forms a complex with CRMP2 and regulates its phosphorylation by cyclin-dependent kinase 5 (Cdk5) at Ser522.[55,58] Collapsin response mediator protein 2 SUMOylation relies on its previous phosphorylation by Cdk5.[23] Although phosphorylated CRMP2 can regulate $Ca_V2.2$ and other ion channels, the SUMOylation of CRMP2 specifically regulates $Na_V1.7$ channels.[11,23] We discovered that increasing CRMP2 deSUMOylation in DRG neurons through CRISPRa-mediated SENP1 overexpression reduces CRMP2 SUMOylation and the $Na_V1.7$–CRMP2 interaction. It also decreases $Na_V1.7$ membrane localization and current density through these channels. Similar results were seen in neuronal CAD cells expressing CRMP2, where co-expression of SENP1 or SENP2 reduced $Na_V1.7$ surface expression and current density through CRMP2 deSUMOylation.[24]

A clear limitation inherent in our study is the fact that CRMP2 does not represent the exclusive target of SENP1.[60,61,69,73] As a result, the observed antinociceptive effect

of SENP1 overexpression may be attributed to its multitarget actions. To address this limitation, we conducted functional assays focusing on 3 proteins known to be modulated by SUMOylation: TRPV1, voltage-gated potassium, and calcium channels. Although these proteins undergo SUMOylation, our findings suggest that other deSUMOylation enzymes, aside from SENP1, likely play a role in mediating this process. For example, previous studies highlighted the involvement of SENP2 in the deSUMOylation of ion channels,[7,14,24,75] thus underscoring the involvement of more than 1 SENP enzyme in regulating channel activity. However, we acknowledge the possibility that SENP1-mediated deSUMOylation could affect other proteins beyond these 3. Further studies will be needed to explore these potential modulations comprehensively.

So far, no SENP1 activators have been reported, but as our data suggest, targeted enhancement of CRMP2 deSUMOylation presents a novel therapeutic pathway for treatment of chronic pain. As a first step toward identification of SENP1 activators, we searched for druggable sites on representative SENP structures and identified a pocket unique to the SENP1 and SENP2 isoforms (Fig. 10). The location of this site is opposite to the interface with SUMO, suggesting that it may be an allosteric site that could be exploited in a virtual screen campaign. Another limitation may be that our behavioral studies revealed a more prolonged anti-allodynic effect with SENP1 overexpression in males when compared to female rats. Databases of deep RNA-sequencing (seq) data revealed that, as opposed to what occurs in female mice with nerve injury, in male mice 4 weeks after SNI, DRG express more *Senp1*.[2] It is plausible that the already increased expression of SENP1 in males contributes to the more prolonged and pronounced antinociceptive effect in comparison to female rats. Although our strategy might not be optimal to use for pain management, what our data highlight is that reduced $Na_V1.7$ currents (not TTX-r currents) because of SENP1 overexpression are at least redundant with CRMP2 deSUMOylation. This is demonstrated using compound **194**[11] (Fig. 9). The mechanism of action of **194** is through direct inhibition of the Ubc9–CRMP2 interaction to prevent the addition of SUMO1 to CRMP2 and specifically control $Na_V1.7$ surface expression and currents.[11] In our electrophysiological recordings, application of **194** did not result in further reduction of sodium current density imposed by SENP1 overexpression, indicating that $Na_V1.7$ currents had been maximally silenced through CRMP2 deSUMOylation.

In conclusion, our results provide proof-of-concept that boosting SENP1 expression and favoring CRMP2 deSUMOylation to decrease $Na_V1.7$ channel function and DRG excitability is an effective means for managing chronic pain. Our data also provide a framework to further develop CRISPRa as a novel and potential tool for chronic pain treatment.

Supplementary Material

Refer to Web version on PubMed Central for supplementary material.

Acknowledgments

This study was supported by the NIH awards from NINDS (NS098772 and NS120663 to R.K.) and NIDA (DA042852 to R.K.).

Sponsorships or competing interests that may be relevant to content are disclosed at the end of this article.

Conflict of interest statement

R.K. is the founder of Regulonix LLC, a company developing nonopioid drugs for chronic pain. In addition, R.K. has patents US10287334 (nonnarcotic CRMP2 peptides targeting sodium channels for chronic pain) and US10441586 (SUMOylation inhibitors and uses thereof) issued to Regulonix LLC.

Data availability statement:

All data are presented in the manuscript or available in the Supplementary Table, available at http://links.lww.com/PAIN/B932.

References

[1]. Agarwal N, Taberner FJ, Rangel Rojas D, Moroni M, Omberbasic D, Njoo C, Andrieux A, Gupta P, Bali KK, Herpel E, Faghihi F, Fleming T, Dejean A, Lechner SG, Nawroth PP, Lewin GR, Kuner R. SUMOylation of enzymes and ion channels in sensory neurons protects against metabolic dysfunction, neuropathy, and sensory loss in diabetes. Neuron 2020;107:1141–59.e7. [PubMed: 32735781]

[2]. Barry AM, Zhao N, Yang X, Bennett DL, Baskozos G. Deep RNA-seq of male and female murine sensory neuron subtypes after nerve injury. PAIN 2023. doi: 10.1097/j.pain.0000000000002934.

[3]. Basbaum AI, Bautista DM, Scherrer G, Julius D. Cellular and molecular mechanisms of pain. Cell 2009;139:267–84. [PubMed: 19837031]

[4]. Becirovic E. Maybe you can turn me on: CRISPRa-based strategies for therapeutic applications. Cell Mol Life Sci 2022;79:130. [PubMed: 35152318]

[5]. Beerli RR, Segal DJ, Dreier B, Barbas CF III. Toward controlling gene expression at will: specific regulation of the erbB-2/HER-2 promoter by using polydactyl zinc finger proteins constructed from modular building blocks. Proc Natl Acad Sci 1998;95:14628–33. [PubMed: 9843940]

[6]. Bennett DL, Clark AJ, Huang J, Waxman SG, Dib-Hajj SD. The role of voltage-gated sodium channels in pain signaling. Physiol Rev 2019;99:1079–151. [PubMed: 30672368]

[7]. Benson MD, Li QJ, Kieckhafer K, Dudek D, Whorton MR, Sunahara RK, Iniguez-Lluhi JA, Martens JR. SUMO modification regulates inactivation of the voltage-gated potassium channel Kv1.5. Proc Natl Acad Sci U S A 2007;104:1805–10. [PubMed: 17261810]

[8]. Black JA, Frézel N, Dib-Hajj SD, Waxman SG. Expression of Nav1.7 in DRG neurons extends from peripheral terminals in the skin to central preterminal branches and terminals in the dorsal horn. Mol Pain 2012;8:82. [PubMed: 23134641]

[9]. Bosmans F, Martin-Eauclaire MF, Swartz KJ. Deconstructing voltage sensor function and pharmacology in sodium channels. Nature 2008;456:202–8. [PubMed: 19005548]

[10]. Brittain JM, Piekarz AD, Wang Y, Kondo T, Cummins TR, Khanna R. An atypical role for collapsin response mediator protein 2 (CRMP-2) in neurotransmitter release via interaction with presynaptic voltage-gated calcium channels. J Biol Chem 2009;284:31375–90. [PubMed: 19755421]

[11]. Cai S, Moutal A, Yu J, Chew LA, Isensee J, Chawla R, Gomez K, Luo S, Zhou Y, Chefdeville A, Madura C, Perez-Miller S, Bellampalli SS, Dorame A, Scott DD, Francois-Moutal L, Shan Z, Woodward T, Gokhale V, Hohmann AG, Vanderah TW, Patek M, Khanna M, Hucho T, Khanna R. Selective targeting of NaV1.7 via inhibition of the CRMP2-Ubc9 interaction reduces pain in rodents. Sci Transl Med 2021;13:eabh1314.

[12]. Chaplan SR, Bach FW, Pogrel JW, Chung JM, Yaksh TL. Quantitative assessment of tactile allodynia in the rat paw. J Neurosci Methods 1994;53:55–63. [PubMed: 7990513]

[13]. Chavez A, Scheiman J, Vora S, Pruitt BW, Tuttle M, P R Iyer E, Lin S, Kiani S, Guzman CD, Wiegand DJ, Ter-Ovanesyan D, Braff JL, Davidsohn N, Housden BE, Perrimon N, Weiss R, Aach J, Collins JJ, Church GM. Highly efficient Cas9-mediated transcriptional programming. Nat Methods 2015;12:326–8. [PubMed: 25730490]

[14]. Chen X, Zhang Y, Ren X, Su Q, Liu Y, Dang X, Qin Y, Yang X, Xing Z, Shen Y, Wang Y, Bai Z, Yeh ETH, Wu H, Qi Y. The SUMO-specific protease SENP2 plays an essential role in the regulation of Kv7.2 and Kv7.3 potassium channels. J Biol Chem 2021;297:101183.

[15]. Cheng J, Kang X, Zhang S, Yeh ET. SUMO-specific protease 1 is essential for stabilization of HIF1α during hypoxia. Cell 2007;131:584–95. [PubMed: 17981124]

[16]. Colasante G, Qiu Y, Massimino L, Di Berardino C, Cornford JH, Snowball A, Weston M, Jones SP, Giannelli S, Lieb A, Schorge S, Kullmann DM, Broccoli V, Lignani G. In vivo CRISPRa decreases seizures and rescues cognitive deficits in a rodent model of epilepsy. Brain 2020;143:891–905. [PubMed: 32129831]

[17]. Dai XQ, Kolic J, Marchi P, Sipione S, Macdonald PE. SUMOylation regulates Kv2.1 and modulates pancreatic beta-cell excitability. J Cell Sci 2009;122:775–9. [PubMed: 19223394]

[18]. Di Maria V, Moindrot M, Ryde M, Bono A, Quintino L, Ledri M. Development and validation of CRISPR activator systems for overexpression of CB1 receptors in neurons. Front Mol Neurosci 2020;13:168. [PubMed: 33013319]

[19]. Dib-Hajj SD, Cummins TR, Black JA, Waxman SG. Sodium channels in normal and pathological pain. Annu Rev Neurosci 2010;33:325–47. [PubMed: 20367448]

[20]. Dib-Hajj SD, Yang Y, Black JA, Waxman SG. The Na(V)1.7 sodium channel: from molecule to man. Nat Rev Neurosci 2013;14:49–62. [PubMed: 23232607]

[21]. Duan JH, Hodgdon KE, Hingtgen CM, Nicol GD. N-type calcium current, Cav2.2, is enhanced in small-diameter sensory neurons isolated from Nf1+/− mice. Neuroscience 2014;270:192–202. [PubMed: 24755485]

[22]. Duran P, Loya-Lopez S, Ran D, Tang C, Calderon-Rivera A, Gomez K, Stratton HJ, Huang S, Xu YM, Wijeratne EMK, Perez-Miller S, Shan Z, Cai S, Gabrielsen AT, Dorame A, Masterson KA, Alsbiei O, Madura CL, Luo G, Moutal A, Streicher J, Zamponi GW, Gunatilaka AAL, Khanna R. The natural product argentatin C attenuates postoperative pain via inhibition of voltage-gated sodium and T-type voltage-gated calcium channels. Br J Pharmacol 2023;180:1267–85. [PubMed: 36245395]

[23]. Dustrude ET, Moutal A, Yang X, Wang Y, Khanna M, Khanna R. Hierarchical CRMP2 posttranslational modifications control NaV1.7 function. Proc Natl Acad Sci U S A 2016;113:E8443–52. [PubMed: 27940916]

[24]. Dustrude ET, Wilson SM, Ju W, Xiao Y, Khanna R. CRMP2 protein SUMOylation modulates NaV1.7 channel trafficking. J Biol Chem 2013;288:24316–31. [PubMed: 23836888]

[25]. Francois-Moutal L, Dustrude ET, Wang Y, Brustovetsky T, Dorame A, Ju W, Moutal A, Perez-Miller S, Brustovetsky N, Gokhale V, Khanna M, Khanna R. Inhibition of the Ubc9 E2 SUMO-conjugating enzyme-CRMP2 interaction decreases NaV1.7 currents and reverses experimental neuropathic pain. PAIN 2018;159:2115–27. [PubMed: 29847471]

[26]. Fukuoka T, Kobayashi K, Yamanaka H, Obata K, Dai Y, Noguchi K. Comparative study of the distribution of the alpha-subunits of voltage-gated sodium channels in normal and axotomized rat dorsal root ganglion neurons. J Comp Neurol 2008;510:188–206. [PubMed: 18615542]

[27]. Garcia-Caballero A, Zhang FX, Chen L, M'Dahoma S, Huang J, Zamponi GW. SUMOylation regulates USP5-Cav3.2 calcium channel interactions. Mol Brain 2019;12:73. [PubMed: 31455361]

[28]. Giehrl-Schwab J, Giesert F, Rauser B, Lao CL, Hembach S, Lefort S, Ibarra IL, Koupourtidou C, Luecken MD, Truong DJ, Fischer-Sternjak J, Masserdotti G, Prakash N, Ninkovic J, Holter SM, Vogt Weisenhorn DM, Theis FJ, Gotz M, Wurst W. Parkinson's disease motor symptoms rescue by CRISPRa-reprogramming astrocytes into GABAergic neurons. EMBO Mol Med 2022;14:e14797.

[29]. Gomez K, Ran D, Madura CL, Moutal A, Khanna R. Non-SUMOylated CRMP2 decreases NaV1.7 currents via the endocytic proteins Numb, Nedd4–2 and Eps15. Mol Brain 2021;14:20. [PubMed: 33478555]

[30]. Halgren TA. Identifying and characterizing binding sites and assessing druggability. J Chem Inf Model 2009;49:377–89. [PubMed: 19434839]

[31]. Hardwick JM, Tse L, Applegren N, Nicholas J, Veliuona MA. The Epstein-Barr virus R transactivator (Rta) contains a complex, potent activation domain with properties different from those of VP16. J Virol 1992;66: 5500–8. [PubMed: 1323708]

[32]. Heckl D, Kowalczyk MS, Yudovich D, Belizaire R, Puram RV, McConkey ME, Thielke A, Aster JC, Regev A, Ebert BL. Generation of mouse models of myeloid malignancy with combinatorial genetic lesions using CRISPR-Cas9 genome editing. Nat Biotechnol 2014;32:941–6. [PubMed: 24952903]

[33]. Hickey CM, Wilson NR, Hochstrasser M. Function and regulation of SUMO proteases. Nat Rev Mol Cell Biol 2012;13:755–66. [PubMed: 23175280]

[34]. Ho Kim S, Mo Chung J. An experimental model for peripheral neuropathy produced by segmental spinal nerve ligation in the rat. PAIN 1992;50:355–63. [PubMed: 1333581]

[35]. Hodgdon KE, Hingtgen CM, Nicol GD. Dorsal root ganglia isolated from Nf1+/− mice exhibit increased levels of mRNA expression of voltage-dependent sodium channels. Neuroscience 2012;206:237–44. [PubMed: 22260870]

[36]. Jia Y, Claessens LA, Vertegaal ACO, Ovaa H. Chemical tools and biochemical assays for SUMO specific proteases (SENPs). ACS Chem Biol 2019;14:2389–95. [PubMed: 31361113]

[37]. Ju W, Li Q, Wilson SM, Brittain JM, Meroueh L, Khanna R. SUMOylation alters CRMP2 regulation of calcium influx in sensory neurons. Channels (Austin) 2013;7:153–9. [PubMed: 23510938]

[38]. Kemaladewi DU, Bassi PS, Erwood S, Al-Basha D, Gawlik KI, Lindsay K, Hyatt E, Kember R, Place KM, Marks RM, Durbeej M, Prescott SA, Ivakine EA, Cohn RD. A mutation-independent approach for muscular dystrophy via upregulation of a modifier gene. Nature 2019;572:125–30. [PubMed: 31341277]

[39]. Khanna R, Yu J, Yang X, Moutal A, Chefdeville A, Gokhale V, Shuja Z, Chew LA, Bellampalli SS, Luo S, Franç ois-Moutal L, Serafini MJ, Ha T, Perez-Miller S, Park KD, Patwardhan AM, Streicher JM, Colecraft HM, Khanna M. Targeting the CaVα-CaVβ interaction yields an antagonist of the N-type CaV2.2 channel with broad antinociceptive efficacy. PAIN 2019;160:1644–61. [PubMed: 30933958]

[40]. Kunz K, Piller T, Muller S. SUMO-specific proteases and isopeptidases of the SENP family at a glance. J Cell Sci 2018;131:jcs211904.

[41]. Legeai JM, Benharkate MM, Duverger JP, Boulu RG. Effects of dihydroergocriptine on mouse and rat resistance to acute anoxia: influence of repetition of treatment. Experientia 1981;37:292–3. [PubMed: 6786914]

[42]. Li Y, De Bolòs A, Amador V, Reverter D. Structural basis for the SUMO2 isoform specificity of SENP7. J Mol Biol 2022;434:167875.

[43]. Liao HK, Hatanaka F, Araoka T, Reddy P, Wu MZ, Sui Y, Yamauchi T, Sakurai M, O'Keefe DD, Nunez-Delicado E, Guillen P, Campistol JM, Wu CJ, Lu LF, Esteban CR, Izpisua Belmonte JC. In Vivo target gene activation via CRISPR/Cas9-Mediated trans-epigenetic modulation. Cell 2017;171:1495–507.e15. [PubMed: 29224783]

[44]. Lima CD, Reverter D. Structure of the human SENP7 catalytic domain and poly-SUMO deconjugation activities for SENP6 and SENP7. J Biol Chem 2008;283:32045–55. [PubMed: 18799455]

[45]. Matharu N, Rattanasopha S, Tamura S, Maliskova L, Wang Y, Bernard A, Hardin A, Eckalbar WL, Vaisse C, Ahituv N. CRISPR-mediated activation of a promoter or enhancer rescues obesity caused by haploinsufficiency. Science 2019;363:eaau0629. [PubMed: 30545847]

[46]. Meents JE, Bressan E, Sontag S, Foerster A, Hautvast P, Rosseler C, Hampl M, Schuler H, Goetzke R, Le TKC, Kleggetveit IP, Le Cann K, Kerth C, Rush AM, Rogers M, Kohl Z, Schmelz M, Wagner W, Jorum E, Namer B, Winner B, Zenke M, Lampert A. The role of Nav1.7 in human nociceptors: insights from human induced pluripotent stem cell-derived sensory neurons of erythromelalgia patients. PAIN 2019;160:1327–41. [PubMed: 30720580]

[47]. Mellert K, Lechner S, Ludeke M, Lamla M, Moller P, Kemkemer R, Scheffzek K, Kaufmann D. Restoring functional neurofibromin by protein transduction. Sci Rep 2018;8:6171. [PubMed: 29670214]

[48]. Meng X, Zheng M, Yu M, Bai W, Zuo L, Bu X, Liu Y, Xia L, Hu J, Liu L, Li J. Transplantation of CRISPRa system engineered IL10-overexpressing bone marrow-derived mesenchymal stem cells for the treatment of myocardial infarction in diabetic mice. J Biol Eng 2019;13:49. [PubMed: 31164920]

[49]. Moutal A, Cai S, Yu J, Stratton HJ, Chefdeville A, Gomez K, Ran D, Madura CL, Boinon L, Soto M, Zhou Y, Shan Z, Chew LA, Rodgers KA, Khanna R. Studies on CRMP2 SUMOylation-deficient transgenic mice identify sex-specific NaV1.7 regulation in the pathogenesis of chronic neuropathic pain. PAIN 2020;161:2629–51. [PubMed: 32569093]

[50]. Moutal A, Chew LA, Yang X, Wang Y, Yeon SK, Telemi E, Meroueh S, Park KD, Shrinivasan R, Gilbraith KB, Qu C, Xie JY, Patwardhan A, Vanderah TW, Khanna M, Porreca F, Khanna R. (S)-lacosamide inhibition of CRMP2 phosphorylation reduces postoperative and neuropathic pain behaviors through distinct classes of sensory neurons identified by constellation pharmacology. PAIN 2016;157:1448–63. [PubMed: 26967696]

[51]. Moutal A, Dustrude ET, Largent-Milnes TM, Vanderah TW, Khanna M, Khanna R. Blocking CRMP2 SUMOylation reverses neuropathic pain. Mol Psychiatry 2018;23:2119–21. [PubMed: 28533518]

[52]. Moutal A, Li W, Wang Y, Ju W, Luo S, Cai S, Francois-Moutal L, Perez-Miller S, Hu J, Dustrude ET, Vanderah TW, Gokhale V, Khanna M, Khanna R. Homology-guided mutational analysis reveals the functional requirements for antinociceptive specificity of collapsin response mediator protein 2-derived peptides. Br J Pharmacol 2018;175:2244–60. [PubMed: 28161890]

[53]. Moutal A, Martin LF, Boinon L, Gomez K, Ran D, Zhou Y, Stratton HJ, Cai S, Luo S, Gonzalez KB, Perez-Miller S, Patwardhan A, Ibrahim MM, Khanna R. SARS-CoV-2 Spike protein co-opts VEGF-A/Neuropilin-1 receptor signaling to induce analgesia. PAIN 2021;162:243–52. [PubMed: 33009246]

[54]. Moutal A, Wang Y, Yang X, Ji Y, Luo S, Dorame A, Bellampalli SS, Chew LA, Cai S, Dustrude ET, Keener JE, Marty MT, Vanderah TW, Khanna R. Dissecting the role of the CRMP2-neurofibromin complex on pain behaviors. PAIN 2017;158:2203–21. [PubMed: 28767512]

[55]. Moutal A, Yang X, Li W, Gilbraith KB, Luo S, Cai S, Francois-Moutal L, Chew LA, Yeon SK, Bellampalli SS, Qu C, Xie JY, Ibrahim MM, Khanna M, Park KD, Porreca F, Khanna R. CRISPR/Cas9 editing of Nf1 gene identifies CRMP2 as a therapeutic target in neurofibromatosis type 1-related pain that is reversed by (S)-Lacosamide. PAIN 2017;158: 2301–19. [PubMed: 28809766]

[56]. Mulcahy JV, Pajouhesh H, Beckley JT, Delwig A, Du Bois J, Hunter JC. Challenges and opportunities for therapeutics targeting the voltage-gated sodium channel isoform Na(V)1.7. J Med Chem 2019;62:8695–710. [PubMed: 31012583]

[57]. O'Shea JM, Perkins ND. Regulation of the RelA (p65) transactivation domain. Biochem Soc Trans 2008;36:603–8. [PubMed: 18631125]

[58]. Patrakitkomjorn S, Kobayashi D, Morikawa T, Wilson MM, Tsubota N, Irie A, Ozawa T, Aoki M, Arimura N, Kaibuchi K, Saya H, Araki N. Neurofibromatosis type 1 (NF1) tumor suppressor, neurofibromin, regulates the neuronal differentiation of PC12 cells via its associating protein, CRMP-2. J Biol Chem 2008;283:9399–413. [PubMed: 18218617]

[59]. Piekarz AD, Due MR, Khanna M, Wang B, Ripsch MS, Wang R, Meroueh SO, Vasko MR, White FA, Khanna R. CRMP-2 peptide mediated decrease of high and low voltage-activated calcium channels, attenuation of nociceptor excitability, and anti-nociception in a model of AIDS therapy-induced painful peripheral neuropathy. Mol Pain 2012;8:54. [PubMed: 22828369]

[60]. Plant LD, Dowdell EJ, Dementieva IS, Marks JD, Goldstein SA. SUMO modification of cell surface Kv2.1 potassium channels regulates the activity of rat hippocampal neurons. J Gen Physiol 2011;137:441–54. [PubMed: 21518833]

[61]. Plant LD, Marks JD, Goldstein SA. SUMOylation of Na(V)1.2 channels mediates the early response to acute hypoxia in central neurons. Elife 2016;5:e20054.

[62]. Reverter D, Lima CD. A basis for SUMO protease specificity provided by analysis of human Senp2 and a Senp2-SUMO complex. Structure 2004;12:1519–31. [PubMed: 15296745]

[63]. Reverter D, Lima CD. Structural basis for SENP2 protease interactions with SUMO precursors and conjugated substrates. Nat Struct Mol Biol 2006;13:1060–8. [PubMed: 17099700]

[64]. Rush AM, Cummins TR, Waxman SG. Multiple sodium channels and their roles in electrogenesis within dorsal root ganglion neurons. J Physiol 2007;579:1–14. [PubMed: 17158175]

[65]. Schmalhofer WA, Calhoun J, Burrows R, Bailey T, Kohler MG, Weinglass AB, Kaczorowski GJ, Garcia ML, Koltzenburg M, Priest BT. ProTx-II, a selective inhibitor of NaV1.7 sodium channels, blocks action potential propagation in nociceptors. Mol Pharmacol 2008;74:1476–84. [PubMed: 18728100]

[66]. Shen L, Tatham MH, Dong C, Zagórska A, Naismith JH, Hay RT. SUMO protease SENP1 induces isomerization of the scissile peptide bond. Nat Struct Mol Biol 2006;13:1069–77. [PubMed: 17099698]

[67]. Shen LN, Liu H, Dong C, Xirodimas D, Naismith JH, Hay RT. Structural basis of NEDD8 ubiquitin discrimination by the deNEDDylating enzyme NEDP1. EMBO J 2005;24:1341–51. [PubMed: 15775960]

[68]. Silveirinha VC, Lin H, Tanifuji S, Mochida S, Cottrell GS, Cimarosti H, Stephens GJ. Ca(V)2.2 (N-type) voltage-gated calcium channels are activated by SUMOylation pathways. Cell Calcium 2021;93:102326.

[69]. Sun H, Lu L, Zuo Y, Wang Y, Jiao Y, Zeng WZ, Huang C, Zhu MX, Zamponi GW, Zhou T, Xu TL, Cheng J, Li Y. Kainate receptor activation induces glycine receptor endocytosis through PKC deSUMOylation. Nat Commun 2014;5:4980. [PubMed: 25236484]

[70]. von Kleist L, Stahlschmidt W, Bulut H, Gromova K, Puchkov D, Robertson MJ, MacGregor KA, Tomilin N, Pechstein A, Chau N, Chircop M, Sakoff J, von Kries J, Saenger W, Krausslich HG, Shupliakov O, Robinson PJ, McCluskey A, Haucke V. Role of the clathrin terminal domain in regulating coated pit dynamics revealed by small molecule inhibition. Cell 2011;146:471–84. [PubMed: 21816279]

[71]. Wang G, Chow RD, Bai Z, Zhu L, Errami Y, Dai X, Dong MB, Ye L, Zhang X, Renauer PA, Park JJ, Shen L, Ye H, Fuchs CS, Chen S. Multiplexed activation of endogenous genes by CRISPRa elicits potent antitumor immunity. Nat Immunol 2019;20:1494–505. [PubMed: 31611701]

[72]. Wang H, Xiong W, Hang S, Wang Y, Zhang S, Liu S. Depletion of SENP1-mediated PPARγ SUMOylation exaggerates intermittent hypoxia-induced cognitive decline by aggravating microglia-mediated neuroinflammation. Aging (Albany NY) 2021;13:15240–54. [PubMed: 34035184]

[73]. Wang Y, Gao Y, Tian Q, Deng Q, Wang Y, Zhou T, Liu Q, Mei K, Wang Y, Liu H, Ma R, Ding Y, Rong W, Cheng J, Yao J, Xu TL, Zhu MX, Li Y. TRPV1 SUMOylation regulates nociceptive signaling in models of inflammatory pain. Nat Commun 2018;9:1529. [PubMed: 29670121]

[74]. Wang Y, Nicol GD, Clapp DW, Hingtgen CM. Sensory neurons from Nf1 haploinsufficient mice exhibit increased excitability. J Neurophysiol 2005;94:3670–6. [PubMed: 16093333]

[75]. Welch MA, Forster LA, Atlas SI, Baro DJ. SUMOylating two distinct sites on the A-type potassium channel, Kv4.2, increases surface expression and decreases current amplitude. Front Mol Neurosci 2019;12:144. [PubMed: 31213982]

[76]. Xiao Y, Blumenthal K, Jackson JO II, Liang S, Cummins TR. The tarantula toxins ProTx-II and huwentoxin-IV differentially interact with human Nav1.7 voltage sensors to inhibit channel activation and inactivation. Mol Pharmacol 2010;78:1124–34. [PubMed: 20855463]

[77]. Xie JY, Chew LA, Yang X, Wang Y, Qu C, Wang Y, Federici LM, Fitz SD, Ripsch MS, Due MR, Moutal A, Khanna M, White FA, Vanderah TW, Johnson PL, Porreca F, Khanna R. Sustained relief of ongoing experimental neuropathic pain by a CRMP2 peptide aptamer with low abuse potential. PAIN 2016;157:2124–40. [PubMed: 27537210]

[78]. Zheng C, Li D, Zhan W, He K, Yang H. Downregulation of SENP1 suppresses LPS-induced macrophage inflammation by elevating Sp3 SUMOylation and disturbing Sp3-NF-κB interaction. Am J Transl Res 2020;12:7439–48. [PubMed: 33312380]

[79]. Zhu X, Zelmer A, Wellmann S. Visualization of protein-protein interaction in nuclear and cytoplasmic fractions by co-immunoprecipitation and in situ proximity ligation assay. J Vis Exp 2017;16:55218.

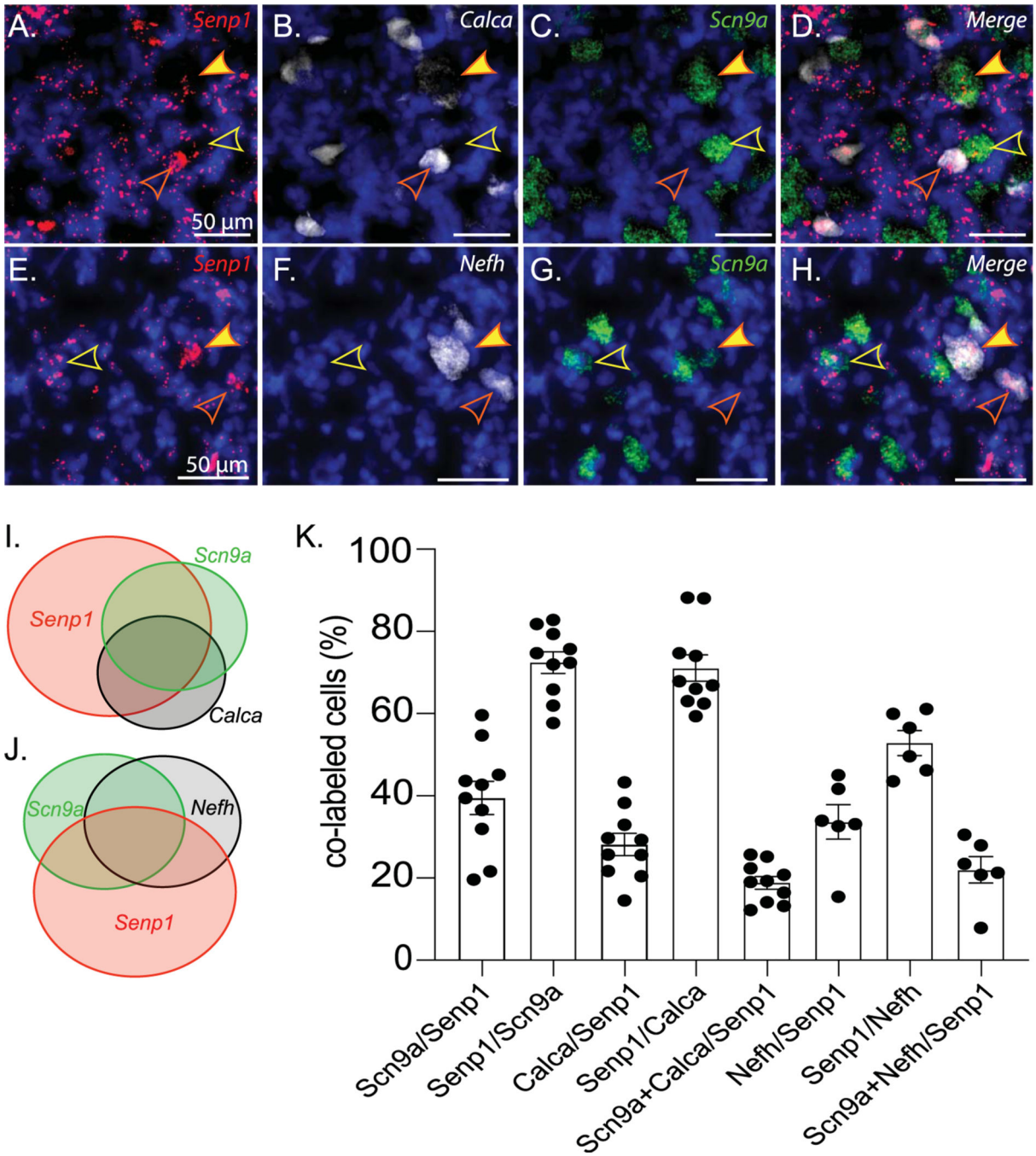

Figure 1.

Senp1 is present in putative nociceptors in the rat dorsal root ganglion. (A–H) Representative images of triple label fluorescence in situ hybridization for *Senp1*, *Scn9a*, *Calca*, and *Nefh* in the lumbar dorsal root ganglion of naive adult rats. In addition, nuclei are labeled with the nuclear labeling dye 49,6-diamidino-2-phenylindole (DAPI). Yellow open arrows indicate *Senp1* and *Scn9a* co-localization, orange open arrows indicate *Nefh*-positive or *Calca*-positive cells with *Senp1* co-localization, and orange arrows with yellow fill indicate triple positive co-localization, respectively. (I and J) Venn diagrams to graphically

illustrate *Senp1*, *Scn9a*, *Calca*, and *Nefh* co-localization. (K) *Senp1* extensively co-localizes with *Scn9a* (*Scn9a/Senp1*: 39.48 ± 4.05%; *Senp1/Scn9a*: 72.42 ± 2.65%), *Calca* (*Calca/Senp1*: 28.16 ± 2.70%; *Senp1/Calca*: 71.06 ± 3.22%), and *Nefh* (*Nefh/Senp1*: 33.65 ± 4.19%; *Senp1/Nefh*: 52.85 ± 3.03%). Furthermore, many *Senp1*-expressing cells co-localize with both *Calca* and *Scn9a* (*Calca* + *Scn9a/Senp1*: 18.85 ± 1.52%) or both *Nefh* and *Scn9a* (*Nefh* + *Scn9a/Senp1*: 21.98 ± 3.23%). n = 10 rats. Individual data points represent the mean of 3 to 5 sections from 2 DRG per individual rat. Scale bars: 100 μm. Error bars indicate mean ± SEM. DRG, dorsal root ganglia.

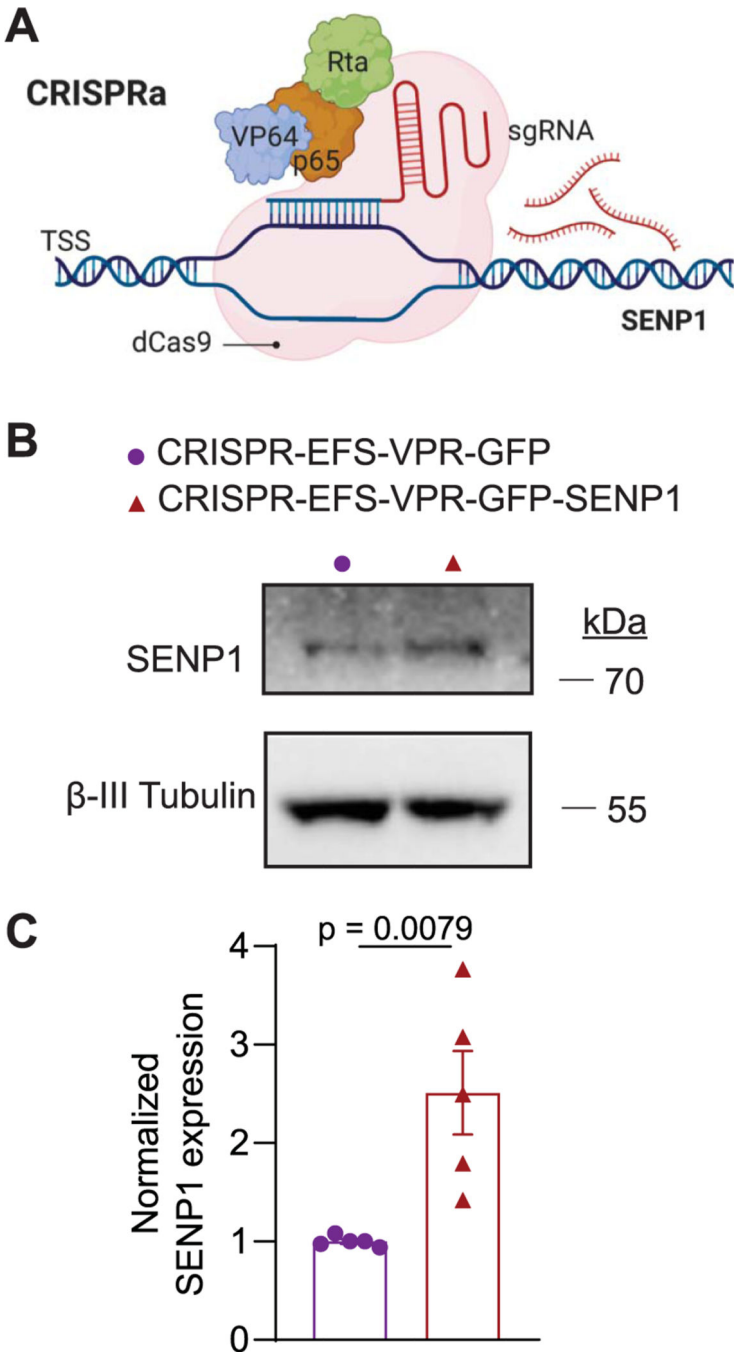

Figure 2.

Validation of SENP1 overexpression in rat dorsal root ganglion neurons through CRISPRa gene editing. (A) In the VPR activation system, dCas9 is fused at the C-terminal end to 3 transcriptional activators (VP64, p65, and Rta). Guide RNAs target upstream of the transcriptional start site (TSS) of the *Senp1* gene, bind the dCas9-VPR, guide the complex to the DNA target site, and then the transcriptional activators are proximal to the TSS for upregulation of the *Senp1* gene. (B) Representative immunoblots showing increased expression of SENP1 in arbitrary units (a.u) after infection with the indicated lentivirus

particles. βIII-Tubulin is used as a loading control. (C) Bar graph with scatter plots showing the quantification of n = 5 samples. *P* values as indicated; Mann–Whitney test; error bars indicate mean ± SEM. For full statistical analyses, see Table S1, available at http://links.lww.com/PAIN/B932. CRISPRa, clustered regularly interspaced short palindromic repeats activation; SENP, Sentrin or SUMO-specific protease; VPR, VP64-p65-Rta.

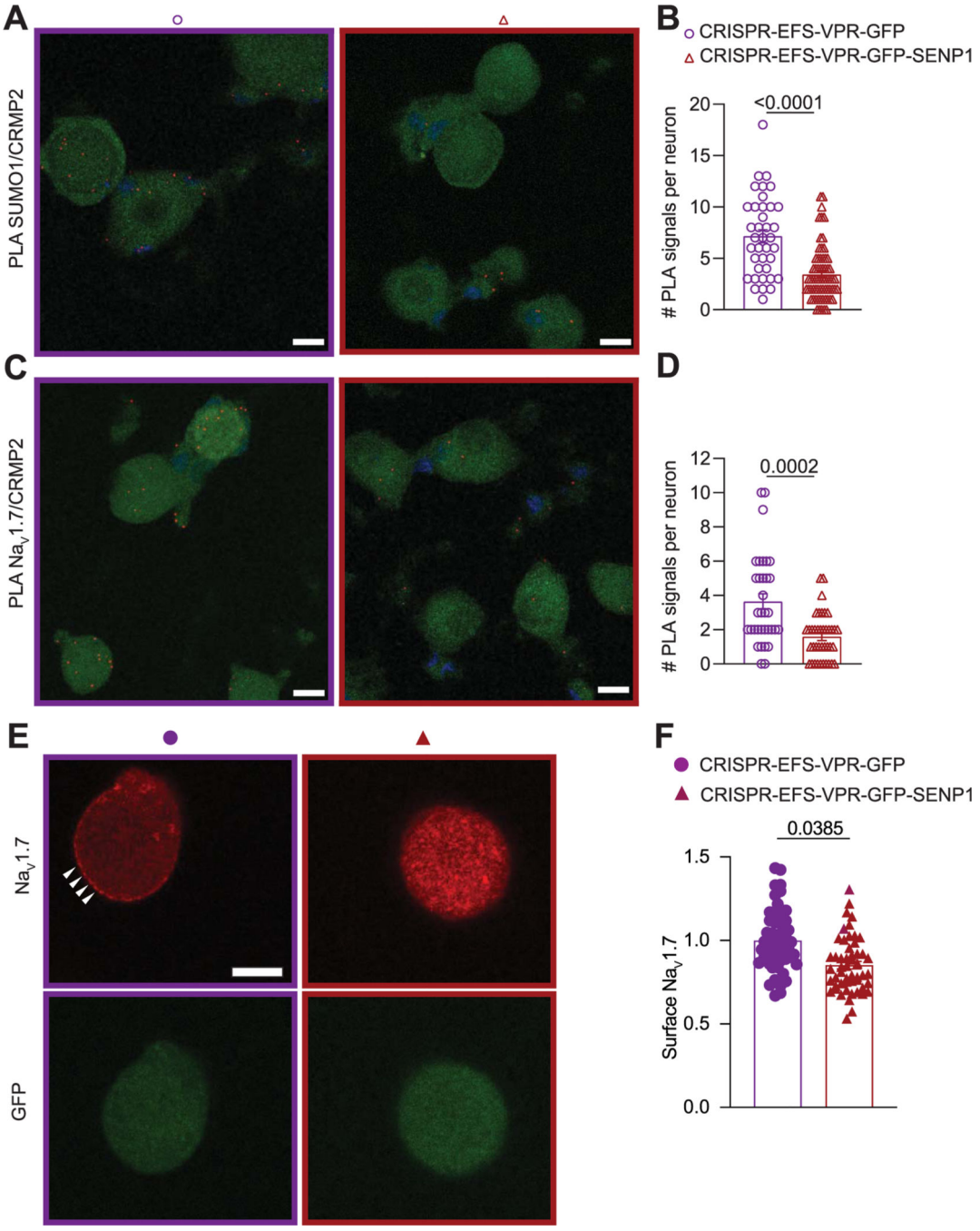

Figure 3.

CRISPRa-mediated SENP1 overexpression reduces SUMO1–CRMP2, Nav1.7–CRMP2 binding, and $Na_V1.7$ surface expression in rat DRG neurons. Representative images of rat DRG cultures transduced with lentiviral particles containing CRISPR-EFS-VPR-GFP (as control) or CRISPR-EFS-VPR-GFP-SENP1 after proximity ligation assay (PLA) between CRMP2 and SUMO1 (A), or between $Na_V1.7$ and CRMP2 (C). GFP signal was used to identify DRG neurons transduced with lentiviral particles. The PLA immunofluorescence labeled sites of interaction between CRMP2 and SUMO1 or $Na_V1.7$ and CRMP2 (red

puncta). In addition, nuclei are labeled with the nuclear-labeling dye 49,6-diamidino-2-phenylindole (DAPI). Scale bar: 10 μm. Quantification of PLA puncta per neuron shows that in DRG neurons transduced with CRISPR-EFS-VPR-GFP-SENP1, SUMO1-CRMP2 (B) and $Na_V1.7$-CRMP2 (D) interactions are significantly reduced compared with CRISPR-EFS-VPR-GFP. n = 34 to 66 cells. *P* values as indicated; Mann–Whitney test; error bars indicate mean ± SEM. (E) Representative confocal images of rat DRG neuron cultures transduced with lentiviral particles containing CRISPR-EFS-VPR-GFP or CRISPR-EFS-VPR-GFP-SENP1 and labeled with an antibody against $Na_V1.7$. GFP signal were used to identify DRG neurons transduced with lentiviral particles. Scale bar: 10 μm. (F) Quantification of normalized surface expression of $Na_V1.7$ per neuron shows that DRG neurons transduced with CRISPR-EFS-VPR-GFP-SENP1 have decreased surface expression of $Na_V1.7$ compared with the control condition. n = 50 to 52 cells; *P* values as indicated; Mann–Whitney test; error bars indicate mean ± SEM. For full statistical analyses, see Table S1, available at http://links.lww.com/PAIN/B932. CRISPRa, clustered regularly interspaced short palindromic repeats activation; CRMP2, collapsin response mediator protein 2; DRG, dorsal root ganglia; SENP, Sentrin or SUMO-specific protease; SUMO, small ubiquitin-like modifier; VPR, VP64-p65-Rta.

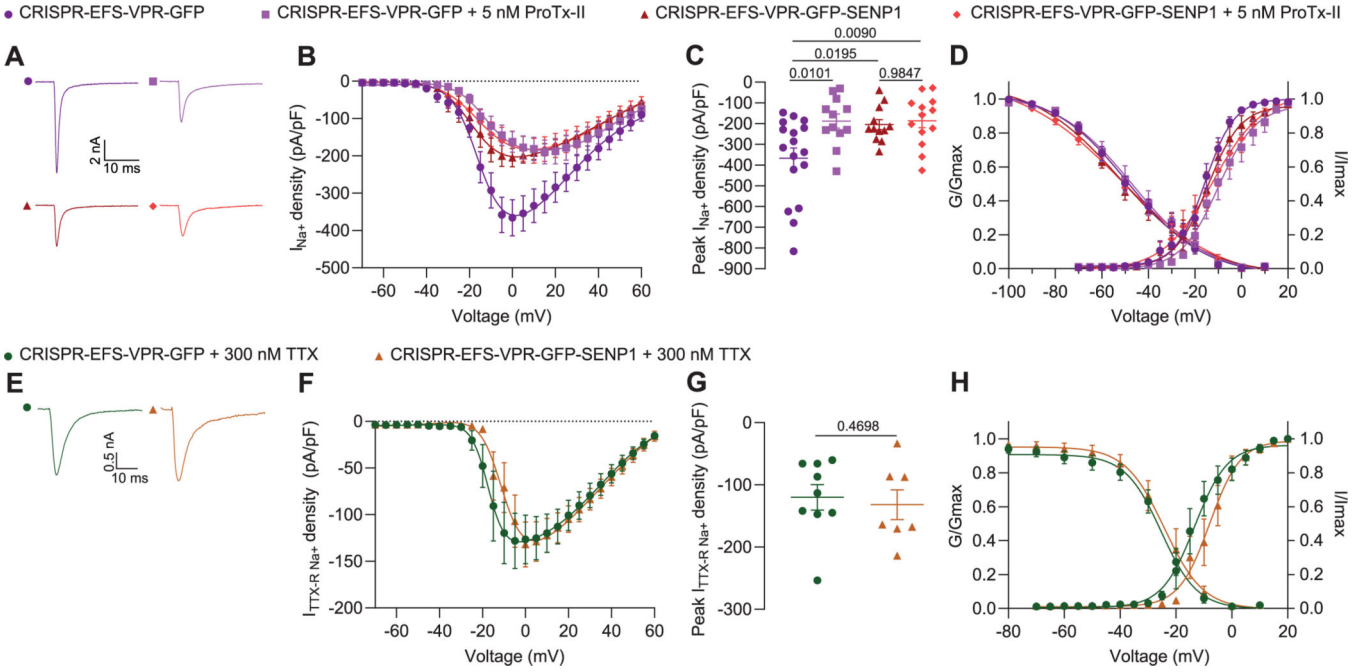

Figure 4.

SENP1 overexpression decreases $Na_V1.7$ currents in sensory neurons. (A) Representative peak sodium current traces obtained from DRG neurons after treatment with CRISPR-EFS-VPR-GFP (as control) or CRISPR-EFS-VPR-GFP-SENP1 lentivirus or compound 48 to 72 hours after infection. (B) Double Boltzmann fits of current density–voltage curves for each of the conditions indicating that overexpression of SENP1 or application of the $Na_V1.7$ channel blocker, ProTx-II (5 nM), decreases sodium currents. (C) Bar graph summary of peak sodium current densities for the indicated conditions showing that ProTx-II (5 nM) does not further decrease sodium currents imposed by CRISPR-EFS-VPR-GFP-SENP1. (D) Boltzmann fits for voltage-dependent activation and inactivation as shown. Half-maximal activation potential of activation and inactivation ($V_{1/2}$) and slope factor values (k) for activation and inactivation are presented in Table 1. *P* values as indicated; 1-way ANOVA followed by Holm–Sidak multiple comparisons test; n = 12 to 17 cells; error bars indicate mean ± SEM. (E) Representative peak TTX-r sodium current traces after DRG infection with the CRISPR-EFS-VPR-GFP or CRISPR-EFS-VPR-GFP-SENP1 48 to 72 hours after infection. (F) Double Boltzmann fits of current density–voltage curves for each of the conditions. (G) Summary bar graph of peak TTX-r sodium current densities for the indicated conditions showing that CRISPR-EFS-VPR-GFP-SENP1 does not alter sodium currents. (H) Boltzmann fits for voltage-dependent activation and inactivation as shown. Half-maximal activation potential of activation and inactivation ($V_{1/2}$) and slope factor values (k) are presented in Table 1. *P* values as indicated; Mann–Whitney test; n = 7 to 9 cells; error bars indicate mean ± SEM. For full statistical analyses, see Table S1, available at http://links.lww.com/PAIN/B932. ANOVA, analysis of variance; CRISPR, clustered regularly interspaced short palindromic repeats; DRG, dorsal root ganglia; SENP, Sentrin or SUMO-specific protease; TTX-r, tetrodotoxin-resistant; VPR, VP64-p65-Rta.

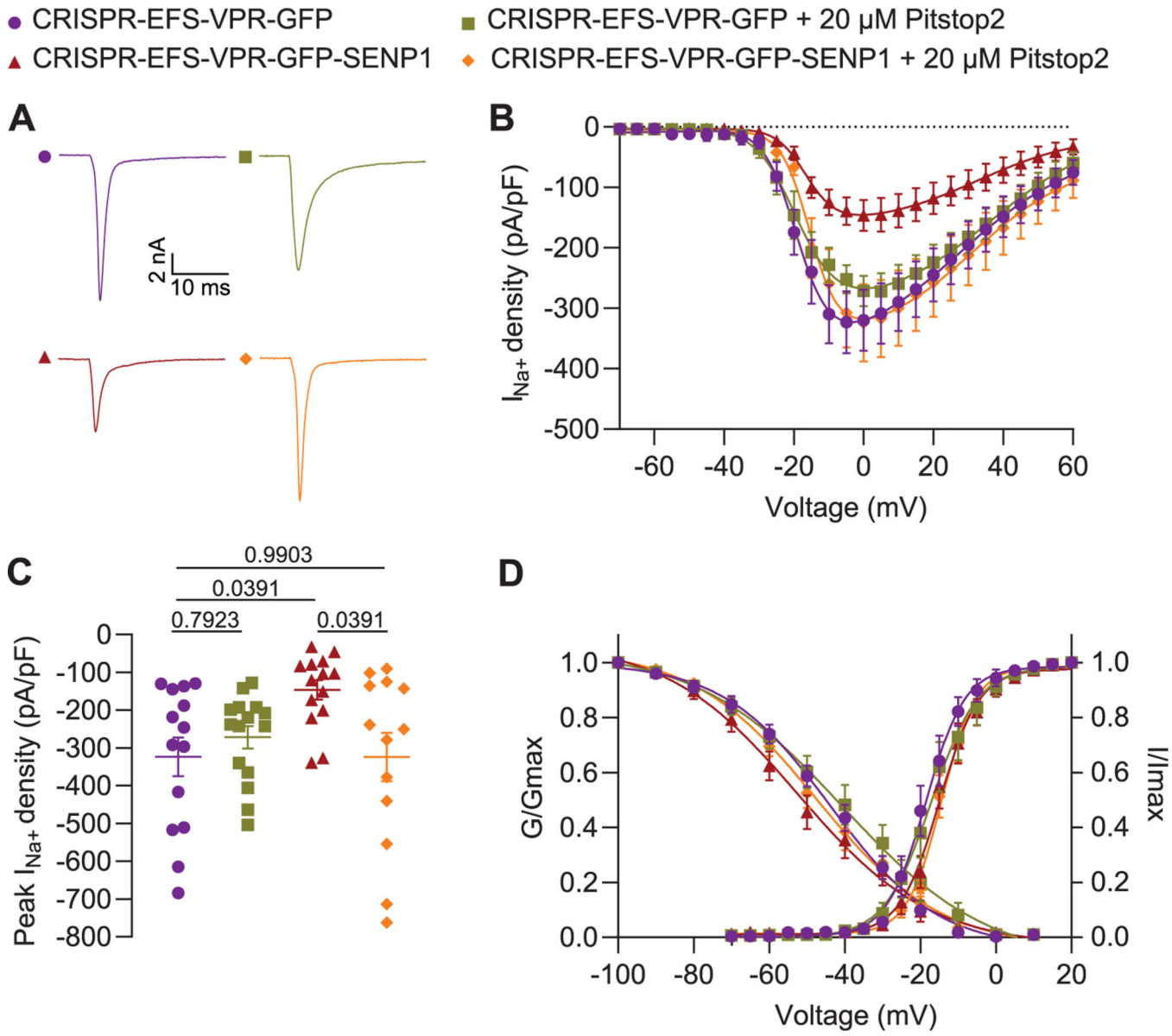

Figure 5.

Reduction of sodium currents induced by SENP1 overexpression is normalized by inhibition of clathrin-mediated endocytosis with Pitstop2. (A) Representative peak sodium current traces after infecting DRG with CRISPR-EFS-VPR-GFP (as control) or CRISPR-EFS-VPR-GFP-SENP1 in the absence or presence of Pitstop2 (20 μM) 48 to 72 hours after infection with lentiviruses. Summary of current density–voltage curves (B) and normalized peak current density (C) from small-sized DRG neurons after a 30-minute incubation with Pitstop2 and infection with the CRISPR-EFS-VPR-GFP or CRISPR-EFS-VPR-GFP-SENP1. (D) Boltzmann fits for voltage-dependent activation and inactivation of the sensory neurons under the indicated conditions. Half-maximal activation and inactivation ($V_{1/2}$) and slope values (k) for activation and inactivation are presented in Table 1. P values as indicated; 1-way ANOVA followed by Holm–Sidak multiple comparisons test; n =

13 to 15 cells; error bars indicate mean ± SEM. For full statistical analyses, see Table S1, available at http://links.lww.com/PAIN/B932. ANOVA, analysis of variance; CRISPR, clustered regularly interspaced short palindromic repeats; DRG, dorsal root ganglia; SENP, Sentrin or SUMO-specific protease; VPR, VP64-p65-Rta.

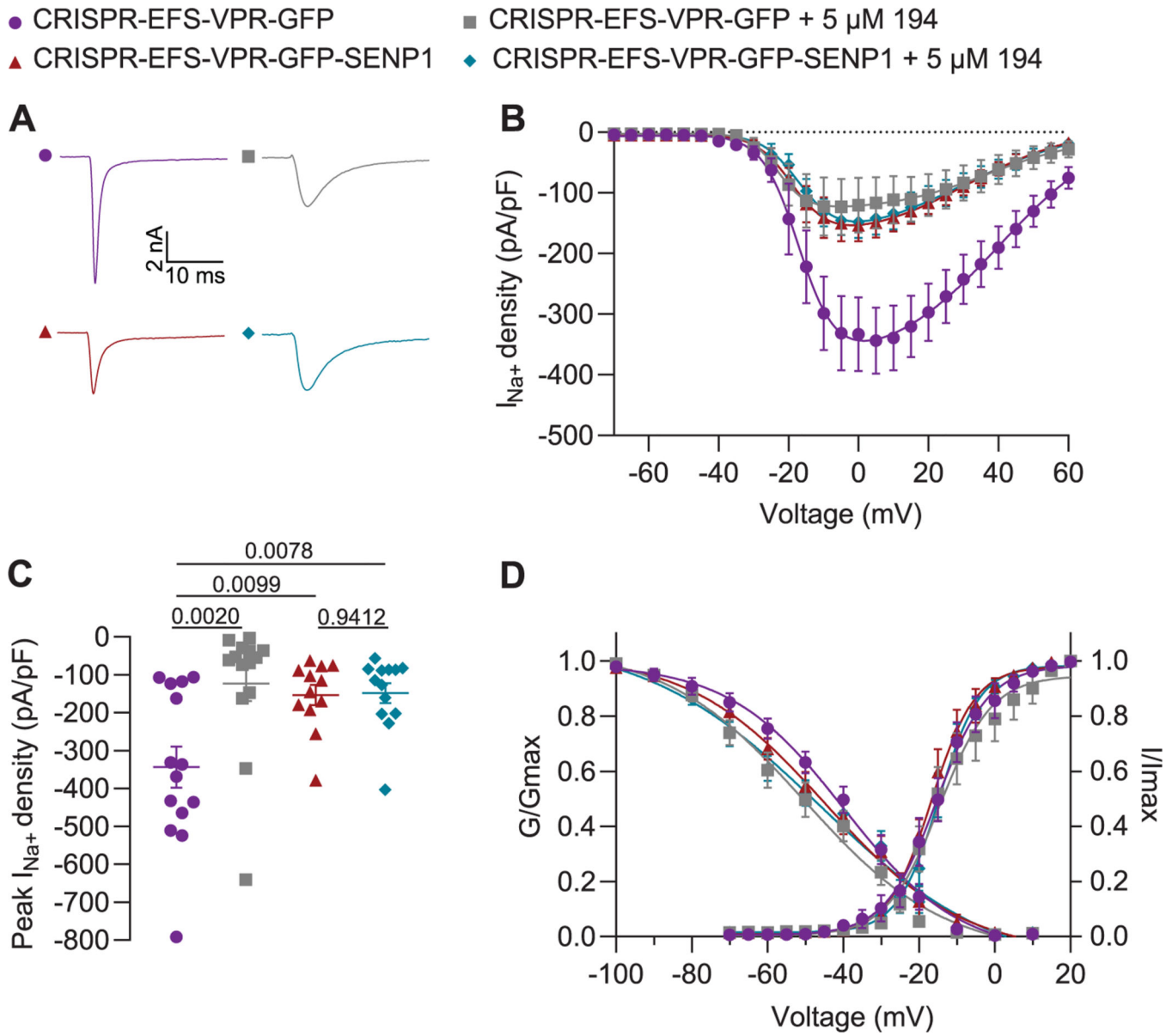

Figure 6.

Reduced sodium currents imposed by SENP1 overexpression are not further affected by pharmacological prevention of CRMP2 SUMOylation with compound **194**. (A) Representative peak current traces recorded from small-sized DRG neurons in the presence and absence of CRISPR-EFS-VPR-GFP-SENP1 or **194** (5 μM). (B) Summary of Boltzmann fits for current density–voltage curves and (C) peak current densities for each of the conditions indicating that overexpression of SENP1 or overnight incubation of **194** (5 μM) decrease sodium currents to the same magnitude. (D) Voltage dependence of activation and inactivation is summarized with Boltzmann fits of normalized conductance (G/Gmax) and currents (I/Imax) Table 1. *P* values as indicated; 1-way ANOVA followed by Holm–Sidak multiple comparisons test; n = 12 to 14 cells; error bars indicate mean ± SEM. For full statistical analyses, see Table S1, available at http://links.lww.com/PAIN/B932. ANOVA,

analysis of variance; CRISPR, clustered regularly interspaced short palindromic repeats; CRMP2, collapsin response mediator protein 2; DRG, dorsal root ganglia; SENP, Sentrin or SUMO-specific protease; SUMO, small ubiquitin-like modifier; VPR, VP64-p65-Rta.

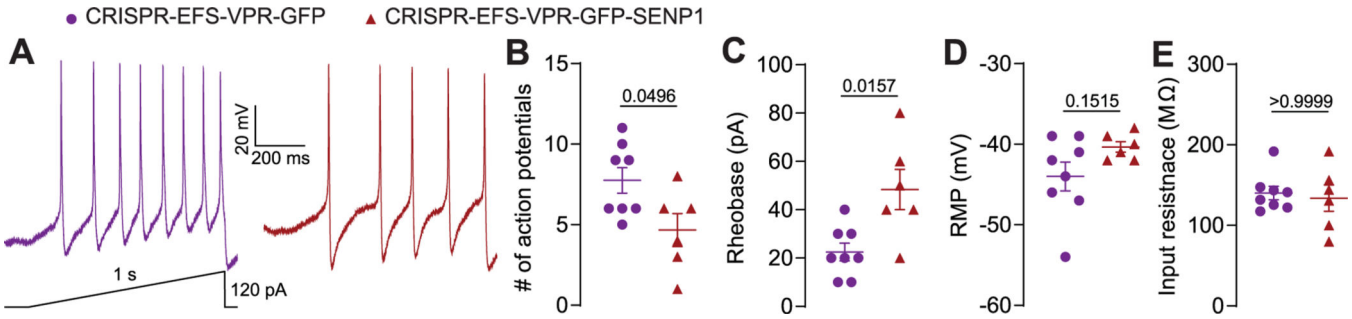

Figure 7.

SENP1 overexpression reduces sensory neuron excitability. (A) Sample traces of action potential (AP) firing in rat DRG neurons infected with CRISPR-EFS-VPR-GFP or CRISPR-EFS-VPR-GFP-SENP1. APs were evoked by injecting a 1-second ramp pulse from 0 to 120 pA. (B) Summary of the number of evoked action potentials in response to a depolarizing ramp stimulus from 0 to 120 pA of current injection. Cells treated with CRISPR-EFS-VPR-GFP-SENP1 are less excitable than cells infected with CRISPR-EFS-VPR-GFP. Quantification of the rheobase (C) in picoamperes (pA), resting membrane potential (D) in millivolts (mV), and input resistance in mega ohms (MΩ) in the indicated conditions. *P* values as indicated; Mann–Whitney test; n = 6 to 8 cells; error bars indicate mean ± SEM. For full statistical analyses, see Table S1, available at http://links.lww.com/PAIN/B932. CRISPR, clustered regularly interspaced short palindromic repeat; DRG, dorsal root ganglia; SENP, Sentrin or SUMO-specific protease; VPR, VP64-p65-Rta.

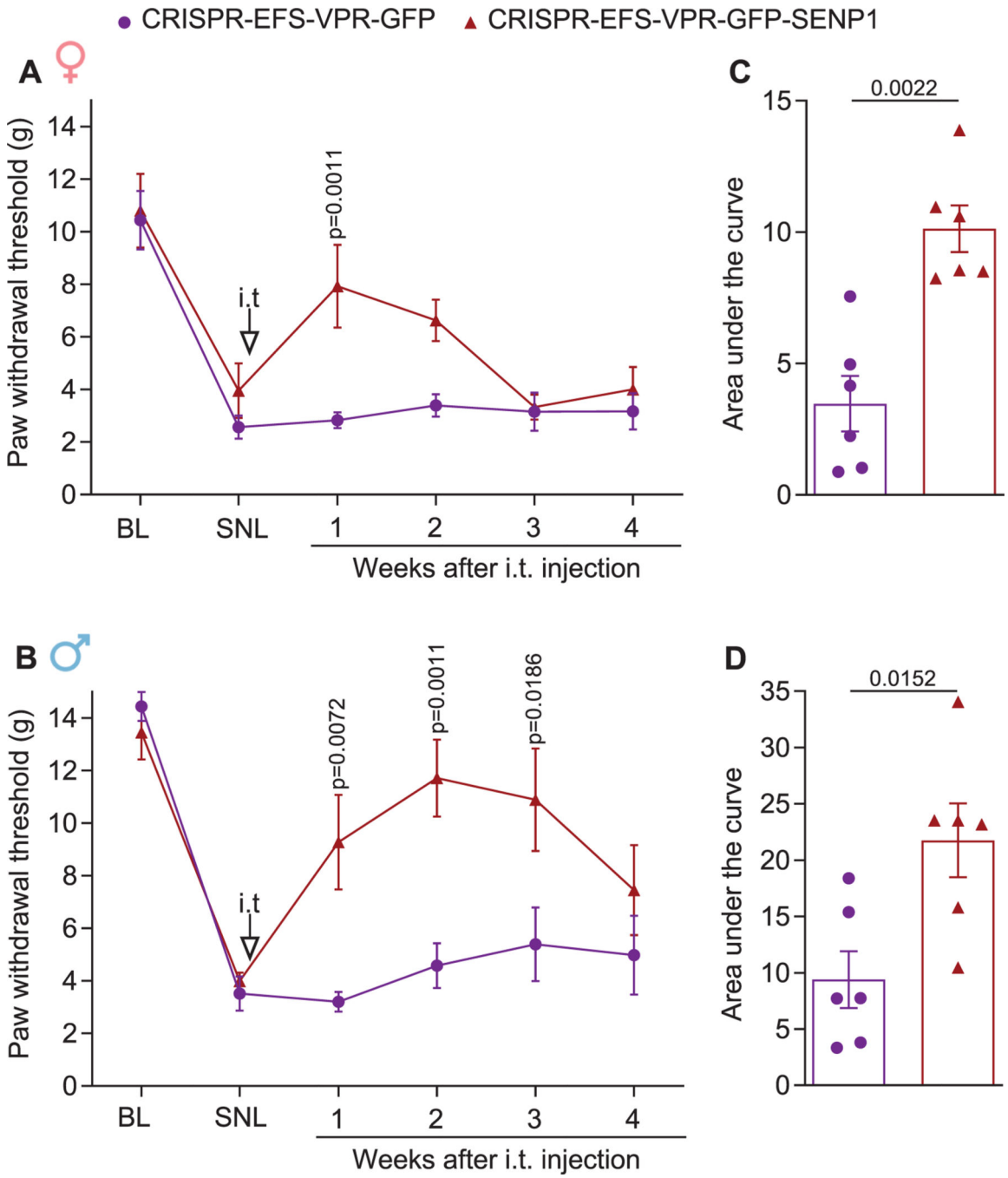

Figure 8.

In vivo overexpression of SENP1 reverses mechanical allodynia after spinal nerve ligation in male and female rats. L5 and L6 spinal nerve ligation (SNL) was performed in male and female rats to induce chronic neuropathic pain. Fourteen days after surgery, animals were administered with CRISPR-EFS-VPR-GFP or CRISPR-EFS-VPR-GFP-SENP1 (~5 × 10^5 IFU/mL in 15 μL) through intrathecal (i.t.) injections. Paw withdrawal thresholds (A, female and B, male) were measured before spinal nerve ligation (baseline; BL), 14 days after surgery (SNL or day 0), and 1, 2, 3, and 4 weeks after intrathecal injection of

lentiviral particles. Panels (C and D) are the area under the curve from 0 (preinjection) to 4 weeks after lentiviral administration. I.t injection of CRISPR-EFS-VPR-GFP-SENP1 had an antinociceptive effect in both male and female rats. *P* values as indicated; paw withdrawal thresholds and latencies were analyzed by 2-way ANOVA, followed by Sidak multiple comparisons test; area under the curve was analyzed by Mann–Whitney test; n = 6 animals; error bars indicate mean ± SEM. For full statistical analyses, see Table S1, available at http://links.lww.com/PAIN/B932. ANOVA, analysis of variance; CRISPR, clustered regularly interspaced short palindromic repeat; DRG, dorsal root ganglia; SENP, Sentrin or SUMO-specific protease; VPR, VP64-p65-Rta.

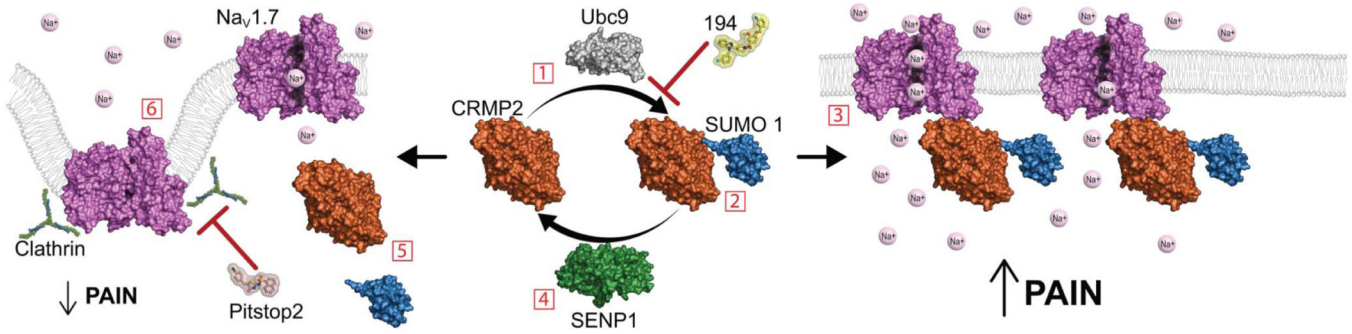

Figure 9.

Schematic representation of CRMP2 regulation of Na$_V$1.7 channels. (1) CRMP2 undergoes Ubc9 SUMOylation (addition of small ubiquitin-like modifiers [SUMOs]) on a lysine residue in position 374. (2) SUMOylation of CRMP2 leads to (3) an increase in Na$_V$1.7–CRMP2 interaction, Na$_V$1.7 channel expression at the plasma membrane, and current influx through these channels, which in turn increases pain sensation. (4) On the other hand, expression of SENP1 (5) promotes CRMP2 deSUMOylation to (6) induce Na$_V$1.7 channel clathrin-mediated endocytosis and decrease pain. Of note, compound **194** prevents addition of SUMO1 to CRMP2 and Pitstop2 inhibits clathrin-mediated endocytosis of Na$_V$1.7. CRMP2, collapsin response mediator protein 2; SENP, Sentrin or SUMO-specific protease.

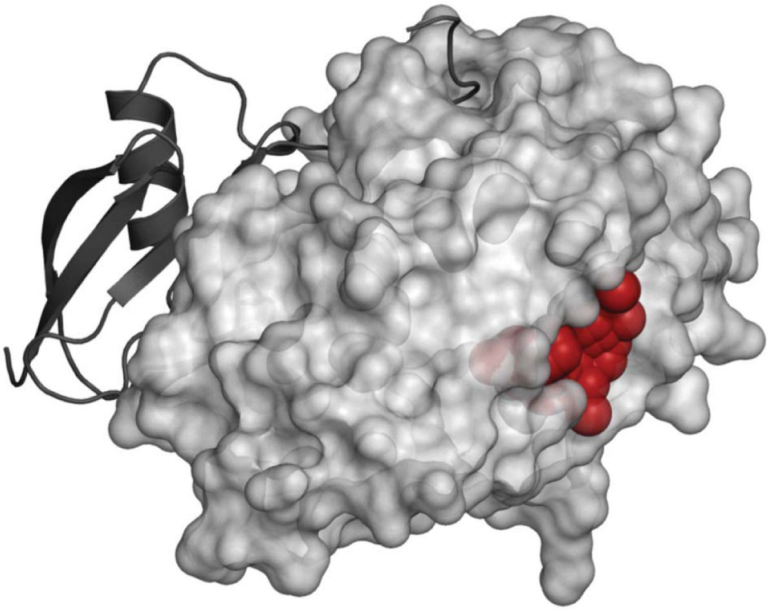

Figure 10.

Potential SENP1 allosteric site. Druggable pocket (red spheres, SiteMap score 0.83) distal to the SUMO interface shown on the structure of SENP1 (light gray surface) with bound SUMO1 precursors (dark gray cartoon), PDB 2iy1.[66] SENP, Sentrin or SUMO-specific protease; SUMO, small ubiquitin-like modifier.

Pain. Author manuscript; available in PMC 2024 September 11.

Table 1

Gating properties and conductance of ionic currents from rat dorsal root ganglion neurons.

Condition (n)	Activation		Inactivation		Conductance
	$V_{1/2}$	k	$V_{1/2}$	k	G
Sodium currents + ProTx-II					
CRISPR-EFS-VPR-GFP (17)	−15.65 ± 0.66	6.37 ± 0.59	−46.68 ± 1.53	−16.35 ± 1.67	104.6 ± 11.35
CRISPR-EFS-VPR-GFP + 5 nM ProTx-II (12)	−9.94 ± 1.33 *	8.03 ± 1.16	−47.00 ± 2.43	−16.25 ± 2.67	65.25 ± 5.61 †
CRISPR-EFS-VPR-GFP-SENP1 (12)	−14.52 ± 1.11	7.11 ± 1.00	−52.21 ± 2.41	−18.53 ± 2.71	60.19 ± 4.62 †
CRISPR-EFS-VPR-GFP-SENP1 + 5 nM ProTx-II (13)	−12.35 ± 2.03	10.67 ± 1.83	−51.66 ± 2.35	−21.48 ± 2.88	70.13 ± 9.30 †
Sodium currents + TTX					
CRISPR-EFS-VPR-GFP (9)	−13.29 ± 0.94	5.85 ± 0.82	−25.27 ± 1.20	−6.43 ± 1.05	44.65 ± 5.71
CRISPR-EFS-VPR-GFP-SENP1 (7)	−7.91 ± 0.92 ‡	5.50 ± 0.80	−24.17 ± 1.57	−6.99 ± 1.39	64.34 ± 13.91
Sodium currents + Pitstop2					
CRISPR-EFS-VPR-GFP (14)	−18.51 ± 0.60	5.17 ± 0.52	−43.84 ± 1.31	−14.25 ± 1.36	109.4 ± 9.92
CRISPR-EFS-VPR-GFP + 20 μM Pitstop2 (15)	−17.10 ± 0.76	6.19 ± 0.67	−40.63 ± 3.08	−19.36 ± 3.67	105.1 ± 10.64
CRISPR-EFS-VPR-GFP-SENP1 (14)	−14.94 ± 0.52	5.21 ± 0.46	−52.54 ± 2.63	−17.55 ± 2.87	68.23 ± 8.79 †
CRISPR-EFS-VPR-GFP-SENP1 + 20 μM Pitstop2 (13)	−14.32 ± 0.39	4.58 ± 0.34	−47.60 ± 1.94	−16.44 ± 2.14	92.10 ± 12.17
Sodium currents + 194					
CRISPR-EFS-VPR-GFP (14)	−15.26 ± 0.85	6.77 ± 0.75	−39.76 ± 1.67	−15.24 ± 1.64	102.6 ± 15.17
CRISPR-EFS-VPR-GFP + 5 μM 194 (14)	−14.54 ± 1.07	6.88 ± 0.95	−50.24 ± 2.18 †	−18.53 ± 2.46	58.34 ± 9.02 †
CRISPR-EFS-VPR-GFP-SENP1 (12)	−16.69 ± 0.61	5.77 ± 0.65	−44.66 ± 2.25	−18.03 ± 2.46	59.37 ± 5.85 †
CRISPR-EFS-VPR-GFP-SENP1 + 5 μM 194 (13)	−14.73 ± 0.53	5.42 ± 0.46	−46.20 ± 2.83	−23.21 ± 3.62	64.69 ± 8.20
I_KA potassium currents					
CRISPR-EFS-VPR-GFP (8)	7.56 ± 5.99	12.62 ± 6.05	−53.54 ± 15.52	−16.01 ± 10.46	50.75 ± 9.24
CRISPR-EFS-VPR-GFP-SENP1 (9)	9.35 ± 5.21	10.81 ± 4.67	−53.52 ± 35.62	−23.13 ± 28.77	47.93 ± 5.47
I_KS potassium currents					
CRISPR-EFS-VPR-GFP (8)	1.45 ± 4.68	13.22 ± 5.35	−31.79 ± 9.10	−21.84 ± 10.39	30.42 ± 7.03

Condition (n)	Activation		Inactivation		Conductance
	$V_{1/2}$	k	$V_{1/2}$	k	G
CRISPR-EFS-VPR-GFP (7)	0.78 ± 1.58	12.68 ± 1.79	−28.09 ± 12.51	−26.63 ± 14.73	48.79 ± 8.39

Values of activation and inactivation properties are mean ± SEM calculated from fits of the data from the indicated number (in parentheses) of cells to the Boltzmann equation. Data were analyzed with 1-way ANOVA with Tukey post hoc test and unpaired *t* test. $V_{1/2}$, midpoint potential (mV) for voltage-dependent activation or inactivation; k, slope factor.

Values of conductance (in picosiemens, pS) are mean ± SEM calculated from the indicated number of cells (in parentheses). Data were analyzed with 1-way ANOVA with Tukey post hoc test and unpaired *t* test. G, conductance.

$^{*}P < 0.001$ CRISPR-EFS-VPR-GFP + 5 nM ProTx-II vs CRISPR-EFS-VPR-GFP, and CRISPR-EFS-VPR-GFP + 5 nM ProTx-II vs CRISPR-EFS-VPR-GFP-SENP1.

$^{\dagger}P < 0.05$ CRISPR-EFS-VPR-GFP + 5 μM 194 vs CRISPR-EFS-VPR-GFP. $P < 0.05$ respect to CRISPR-EFS-VPR-GFP.

$^{\ddagger}P < 0.05$ CRISPR-EFS-VPR-GFP vs CRISPR-EFS-VPR-GFP-SENP1.

ANOVA, analysis of variance; CRISPR, clustered regularly interspaced short palindromic repeats; TTX, tetrodotoxin; VPR, VP64-p65-Rta.

Table 2

Inactivation time constants (τ) of sodium currents.

Condition (n)	τ (ms)							
	−50 mV	−40 mV	−30 mV	−20 mV	−10 mV	0 mV	10 mV	20 mV
Sodium currents + ProTx-II								
CRISPR-EFS-VPR-GFP (17)	36.57 ± 7.10	21.92 ± 7.33	7.49 ± 1.58	6.53 ± 1.78	4.25 ± 0.89	3.98 ± 0.51	3.94 ± 0.55	3.33 ± 0.61
CRISPR-EFS-VPR-GFP + 5 nM ProTx-II (12)	47.08 ± 11.35	27.66 ± 4.04	18.62 ± 5.75	14.45 ± 5.62	6.11 ± 1.51	5.65 ± 1.07	4.55 ± 0.53	3.79 ± 0.46
CRISPR-EFS-VPR-GFP-SENP1 (12)	24.98 ± 6.35	13.01 ± 3.09	5.98 ± 1.25	6.56 ± 1.64	3.53 ± 0.65	3.55 ± 0.65	3.24 ± 0.58	2.53 ± 0.50
CRISPR-EFS-VPR-GFP-SENP1 + 5 nM ProTx-II (13)	29.51 ± 5.46	19.95 ± 5.24	7.33 ± 1.62	6.21 ± 2.08	5.91 ± 2.37	5.53 ± 1.51	4.84 ± 0.98	4.07 ± 0.85
Sodium currents + Pitstop2								
CRISPR-EFS-VPR-GFP (14)	67.20 ± 57.58	23.89 ± 17.01	15.53 ± 2.94	6.89 ± 5.79	5.46 ± 2.46	5.44 ± 2.01	5.95 ± 5.36	1.75 ± 3.92
CRISPR-EFS-VPR-GFP 1 20 μM Pitstop2 (15)	20.21 ± 13.29	18.25 ± 14.33	11.55 ± 8.24	8.85 ± 10.66	5.99 ± 5.03	5.78 ± 5.02	5.96 ± 5.43	5.09 ± 5.22
CRISPR-EFS-VPR-GFP-SENP1 (14)	35.72 ± 33.93	17.65 ± 11.32	19.42 ± 16.77	11.36 ± 12.21	4.83 ± 2.65	4.49 ± 2.29	6.62 ± 5.05	8.64 ± 7.93
CRISPR-EFS-VPR-GFP-SENP1 + 20 μM Pitstop2 (13)	26.48 ± 21.51	17.83 ± 19.46	17.71 ± 24.80	9.27 ± 8.79	4.28 ± 2.16	4.28 ± 1.82	3.84 ± 1.59	4.41 ± 2.40
Sodium currents + 194								
CRISPR-EFS-VPR-GFP (14)	74.86 ± 22.98	39.26 ± 15.62	20.46 ± 6.67	12.43 ± 3.24	6.77 ± 2.06	5.56 ± 1.40	4.97 ± 1.20	3.12 ± 0.8
CRISPR-EFS-VPR-GFP + 5 μM 194 (14)	107.64 ± 27.82	89.58 ± 22.62	40.37 ± 11.56	28.27 ± 15.79	7.13 ± 2.25	9.37 ± 4.21	4.05 ± 1.26	2.61 ± 0.93
CRISPR-EFS-VPR-GFP-SENP1 (12)	62.45 ± 9.98	54.12 ± 10.84	29.41 ± 10.58	6.31 ± 1.68	5.77 ± 0.84	4.35 ± 0.75	3.64 ± 0.45	2.65 ± 0.33
CRISPR-EFS-VPR-GFP-SENP1 + 5 μM 194 (13)	65.05 ± 18.89	75.24 ± 27.52	33.70 ± 12.08	10.67 ± 4.19	4.38 ± 0.61	5.27 ± 1.12	3.17 ± 0.61	2.02 ± 0.44
Condition (n)	**τ (ms)**							
	−30 mV	**−20 mV**	**−10 mV**	**0 mV**	**10 mV**	**20 mV**	**30 mV**	**40 mV**
Sodium currents + TTX								
CRISPR-EFS-VPR-GFP (9)	44.28 ± 22.92	26.74 ± 9.56	11.33 ± 5.26	6.87 ± 1.10	4.95 ± 1.38	3.91 ± 1.26	3.93 ± 1.62	3.59 ± 1.26
CRISPR-EFS-VPR-GFP-SENP1 (7)	33.57 ± 12.85	17.66 ± 7.72	7.36 ± 3.32	5.15 ± 1.60	5.09 ± 1.57	3.89 ± 1.25	2.78 ± 0.944	1.68 ± 0.72

Values are mean ± SEM calculated from the data from the indicated number (in parentheses) of cells. Data were analyzed with 2-way ANOVA with Holm–Sidak multiple comparisons test and multiple *t* test. No statistical differences were observed.

ANOVA, analysis of variance; CRISPR, clustered regularly interspaced short palindromic repeat; SENP, Sentrin or SUMO-specific protease; TTX, tetrodotoxin; VPR, VP64-p65-Rta.